FEARC-00-001

STRESSES IN BONDED REPAIR TO CYLINDRICALLY CURVED SHELL STRUCTURES

Liyong Tong and Xiannian Sun

Department of Aeronautical Engineering, The University of Sydney

New South Wales 2006 AUSTRALIA

REPORT DOCUMENTATION PAGE

Form Approved OMB No. 074-0188

1. AGENCY USE ONLY (Leave blank)	2. REPORT DATE	3. REPORT TYPE AND DATES COVERED
	June 16, 2000	Final and 1 Jun 1999 - 31 May 2000

4. TITLE AND SUBTITLE
Stresses in bonded repair to cylindrically curved shell structures

5. FUNDING NUMBERS
C ~~F6256200M9108~~
F6256299M9126

6. AUTHOR(S)
Liyong Tong and Xiannian Sun

7. PERFORMING ORGANIZATION NAME(S) AND ADDRESS(ES)
Department of Aeronautical Engineering
University of Sydney
New South Wales 2006
Australia

8. PERFORMING ORGANIZATION REPORT NUMBER
FEARC-00-001

9. SPONSORING / MONITORING AGENCY NAME(S) AND ADDRESS(ES)
Air Force Research Laboratory,
AFOSR/AOARD
7-23-17 Roppongi
Minato-ku, Tokyo 106-0032, Japan

10. SPONSORING / MONITORING AGENCY REPORT NUMBER

11. SUPPLEMENTARY NOTES

12a. DISTRIBUTION / AVAILABILITY STATEMENT
DISTRIBUTION STATEMENT A
Approved for Public Release
Distribution Unlimited

12b. DISTRIBUTION CODE

13. ABSTRACT ***(Maximum 200 Words)***

Adhesive bonding has been used to join or repair metallic and composite structural components to achieve or restore their designated structural stiffness and strengths. However, current analysis methods and empirical databases for composite bonded joint design and for composite bonded patch repair are limited to flat plate and/or flat laminate geometries, and the effect of curvature on the performance and durability of composite bonded joints and repairs is not known. This report presents a novel finite element formulation for developing adhesive elements for conducting 2.5-D quick stress analysis of bonded repairs to curved structures. Both large deflections of the parent structures and nonlinear adhesive behavior are incorporated in the formulation. An in-house software called BPATCH has been developed. A variety of examples are presented to illustrate the effect of curvature, large deflection and adhesive nonlinear behavior on stresses in adhesive layer. Illustrative examples also indicate the effect of patch location, i.e., internal and external patches, patch size and patch thickness.

14. SUBJECT TERMS	15. NUMBER OF PAGES
Bonded repair, curvature effect, finite element method, stresses	78
	16. PRICE CODE

17. SECURITY CLASSIFICATION OF REPORT	18. SECURITY CLASSIFICATION OF THIS PAGE	19. SECURITY CLASSIFICATION OF ABSTRACT	20. LIMITATION OF ABSTRACT
Unclassified	Unclassified	Unclassified	SAR

ABSTRACT

Adhesive bonding has been used to join or repair metallic and composite structural components to achieve or restore their designated structural stiffness and strengths. However, current analysis methods and empirical databases for composite bonded joint design and for composite bonded patch repair are limited to flat plate and/or flat laminate geometries, and the effect of curvature on the performance and durability of composite bonded joints and repairs is not known. This report presents a novel finite element formulation for developing adhesive elements for conducting 2.5-D quick stress analysis of bonded repairs to curved structures. Both large deflections of the parent structures and nonlinear adhesive behavior are incorporated in the formulation. An in-house software called BPATCH has also been developed. A variety of examples are presented to illustrate the effect of curvature, large deflection and adhesive nonlinear behavior on stresses in adhesive layer. Illustrative examples also indicate the effect of patch location, i.e., internal and external patches, patch size and patch thickness.

TABLE OF CONTENTS

1. INTRODUCTION

Adhesive-bonded patching is one of the most widely used repairing techniques to cracked or damaged metallic and composite structures [1,2]. In this technique; a composite patch is bonded to the parent structure to reinforce the cracked zone [3] and to try to restore the structure to its original design specifications. This technique has successfully addressed some of the aging aircraft problem [1], and there exists a large number of research publications available on analysis, testing and design of adhesive-bonded patching repairs. To successfully apply this technique to practical problems, one needs to consider many aspects of this technique, for example, stress analysis, static and fatigue strength, surface preparation, selection of adhesives, durability, etc. One important aspect in designing a bonded patch is stress analysis and strength prediction. As a bonded patch is similar to an adhesive-bonded joint, the concepts and methodologies developed for analyzing stresses in bonded joints can be readily applied to conducting stress calculation for a bonded patch. There is a large amount of information on stress analysis of the bonded joints and repairs in the literature. Most of the currently available analysis methods and empirical databases for composite bonded joint design and for composite patch repair designs are limited to flat plate and/or flat laminate geometries [1, 4-6]. However, in addition to flat panels, curved panels or shell-type structures are widely used in the design of metallic and composite structures. Comparing to the knowledge of bonded joints/repairs to flat surfaces, current knowledge on the effect of curvature(s) on the performance and durability of composite bonded joints and bonded composite repairs is extremely limited. For example, the effect of curvature(s) on the interlaminar stresses resulting from residual curing stresses and thermo-mechanical loading has not been determined. It has been demonstrated in numerous programs over many years that the critical interlaminar stresses govern the lifetime performance of adhesive joints and current analysis tools for designing bonded joints for flat geometries focus on minimizing interlaminar stresses to maximize the joint durability. The overall objective of this research effort is towards development of validated new analysis methodologies for designing high-performance and durable bonded joints and/or repairs to curved surfaces. In this report, current concepts and methodologies used in bonded joints and repairs are extended to take into account the effect of curvature on stresses in adhesive layer.

Stresses in adhesive layer can be determined following two types of solution procedures, namely, analytical and numerical analysis procedures. In the analytical procedure, closed-

form solutions for stresses may be obtained, while in the numerical analysis procedure, finite element method is widely used. In general, analytical solutions are limited to simple geometrical configurations and material properties, while finite element method is more versatile in terms of geometrical configuration and material properties, thus theoretically speaking, it can be applied to solve most of the joints and repairs problems. In finite element analysis, it is desirable to conduct a full 3-D analysis to obtain an accurate and detailed stress information. However, a full 3-D analysis involves detailed modeling of adhesive layer and parent structures. In a typical 3-D analysis, brick elements are used to model the thin-walled structures, patches and adhesive layer and fine mesh with small size elements of the order of adhesive thickness must be used to maintain an appropriate aspect ratio and to obtain reasonable accurate numerical solutions. Thus it can be extremely expensive, and may become even impossible under certain circumstances. It is desirable to develop a simple, efficient and cost-effective theoretical framework using simple adhesive elements to capture the main features of stresses in the adhesive layer, to take into account the effect of curvature and to enable an engineer to conduct a reliable quick design.

In this report, the effect of curvature on both peel and shear stresses in adhesive layer in adhesive-bonded curved patches has been presented. By assuming constant peel and shear strains across adhesive thickness, a new finite element formulation has been proposed for developing an 8-node adhesive element which can be used to calculate stresses in adhesive layer. In the new formulation, the bonded overlap is modeled as a sandwich type of structure and the strain energy of the adhesive layer is considered in terms of the nodal displacements and rotations of the two adjacent 4-node flat shell elements. Some illustrative examples are presented to demonstrate the effect of curvature on peak peel and shear stresses in the adhesive layer under selected loading and boundary conditions.

2. PROBLEM STATEMENT AND BASIC ASSUMPTIONS

A cracked or damaged thin-walled structure can be reinforced from either side of the structure by bonding a composite thin patch. When only one patch is bonded to one side of the structure it is referred to as single-sided bonded repair, when two patches are bonded to both sides of the structure it is referred to as double-sided bonded repair. Selection of single-sided or double-sided bonded repair depends on many factors, such as accessibility to either side of thin-walled structure, design requirements and stress environments etc. In this report we only consider single-sided bonded repairs to thin-walled structures.

A significant amount of research has been performed in modeling adhesive bonded repairs to flat surfaces [1-3] using one-, two- or three-dimensional approaches. Although three-dimensional approaches are more accurate than two-dimensional theories, their implementation can be very expensive for practical applications. Thus in this research program, a two-dimensional theory for adhesive bonded repairs to cylindrically curved shell structures will be developed first to provide a general framework for accurate and computationally efficient analysis.

Similar to a structural bonded joint [5,6], the adhesive layer in a bonded repair is often very thin and non-uniform due to primarily lack of technologies for accurate control of bondline thickness in manufacturing structural components. To model the behavior of an adhesive layer, it is assumed that the patch is perfectly bonded to the thin-walled structure, the adhesive thickness is uniform over the entire bonding area, and the adhesive layer is very thin and very flexible comparing to these of the patch and thin-walled structures. This is a widely accepted assumption in analysis of structural bonded joints [5,6].

The second assumption is concerned with the stresses in adhesive layer. It is assumed that the three in-plane stresses in the adhesive layer are extremely small comparing to the other three out-of-plane stress components so that they can be neglected. Thus only the normal or peel stress σ_{zz} and the two out-of-plane shear stresses τ_{yz} and τ_{xz} are taken into account in the problem formulation. They are assumed to be constant across the adhesive thickness. This assumption is a natural extension of that widely used in adhesive bonded joints and/or repairs to flat surfaces or plates [1-2,5-6]. This assumption enables us to establish the

relations between the adhesive strain components and the mid-plane displacements and rotations of the parent shell structures and the bonded patches.

The third assumption is that the thin-walled parent structure and bonded patches can be modeled using the well-known the first-order or moderately thick plate and shell theory. The selection of the first-order thick plate and shell theory is due to the fact that transverse shear deformations play an important in composite patches or plates and shells. Based one the first-order plate and shell theory, all displacements in any point of the plate or shell can be determined using the three translational and three rotational deformations on the middle or neutral plane. In particular, the three displacements on both surfaces of the plates and shells or patches can be expressed in terms of the three translations and two rotations. This assumption is a natural extension of those adopted in simplified analysis of all types of lap joints [6].

Application of the above assumptions enables us to model the bonded patch to a thin-walled structure as a structure with two plates or shells sandwiching an adhesive layer, which only is subject to the three out-of-plane strains and stresses. Comparing to a full 3-D finite element modeling scheme, which models both parent thin-walled structures and bonded patches as well as adhesive layer using brick elements, the current scheme uses plate and shell elements and pseudo-brick elements for adhesive layer, and is referred to as a 2.5-D finite element analysis.

3. FUNDAMENTAL FORMULATION OF ADHESIVE ELEMENT

The assumptions described in Section 2 are used to develop the fundamental formulation for adhesive element for conducting 2.5-D finite element analysis of bonded repairs. In this section, a variational functional will be presented and then used to develop a theoretical framework for constructing adhesive elements.

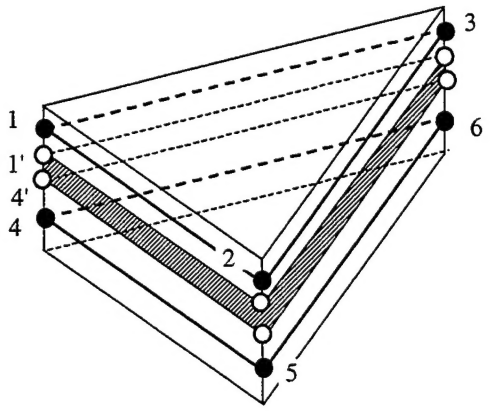

Figure 3-1 Schematic of a 6-node adhesive element

3.1. Definition of adhesive element

In this report, an adhesive element is defined as an element that comprises of one pseudo-brick adhesive element and two plate or shell elements. The two plate and shell elements are located on either side of the adhesive layer and offset by half thickness of the corresponding wall thickness of the element. Both plate and shell elements must have the same number of nodes to form the node pairs. At each node pair, the two plate and shell elements share the same normal, or in other words, the two nodes must locate on the normal of the element. Figure 3-1 depicts an adhesive element to illustrate the definition and limitation. As shown in this figure, there are three node pairs, i.e., node 1 and 4, node 2 and 5, and node 3 and 6 as represented by solid circles. As the 3-node plate element is a flat one, the two elements must have the same normal to their middle planes. Node 1 and 4 must be located along the normal passing through node 1 or 4. The hollow circles represent the pseudo nodes of the pseudo brick element for adhesive layer, and they are dependent on the corresponding nodes of the plate and shell elements. For example, pseudo node 1' is dependent on node 1.

Introduction of this restrictions in node numbering and geometry makes it possible to incorporate the adhesive element into the commercially available software and makes it an easy and convenient job to generate meshes, particularly in the bonded area, for building up finite element analysis models. With such restrictions, it is still possible to model non-uniform thickness of adhesive and plates or shells by using different thickness configurations of adjacent elements.

3.2. Variational formulation

For a thin-walled structure with a bonded repair, the total strain energy of the system can be divided into the following two parts: (a) strain energy due to deformation of the upper and lower shell element; and (b) strain energy due to deformation of adhesive layer. The formulations for these strain energy terms are given as follows:

(a) Strain energy in the thin-walled structure U_u and the bonded patch U_l;

For an adhesive element, using the first-order plate and shell theory (Reissner-Mindlin theory), the strain energy terms U_u and U_l can be given by

$$U_k = \frac{1}{2}\int_{\text{Element area}} \begin{Bmatrix} \varepsilon_m^k & \varepsilon_b^k & \varepsilon_s^k \end{Bmatrix} [D^k] \begin{Bmatrix} \varepsilon_m^k \\ \varepsilon_b^k \\ \varepsilon_s^k \end{Bmatrix} dA$$

$$= \frac{1}{2}\int_{\text{Element area}} \begin{Bmatrix} \varepsilon_m^k & \varepsilon_b^k & \varepsilon_s^k \end{Bmatrix} \begin{bmatrix} A^k & B^k & 0 \\ B^k & D^k & 0 \\ 0 & 0 & H^k \end{bmatrix} \begin{Bmatrix} \varepsilon_m^k \\ \varepsilon_b^k \\ \varepsilon_s^k \end{Bmatrix} dA \qquad (k= u, l) \qquad (1)$$

where

$$\varepsilon_m^k = \begin{Bmatrix} \varepsilon_{xx}^{0k} \\ \varepsilon_{yy}^{0k} \\ \gamma_{xy}^{0k} \end{Bmatrix}, \qquad \varepsilon_b^k = \begin{Bmatrix} k_{xx}^{0k} \\ k_{yy}^{0k} \\ k_{xy}^{0k} \end{Bmatrix}, \qquad \varepsilon_s^k = \begin{Bmatrix} \gamma_{yz}^k \\ \gamma_{xz}^k \end{Bmatrix} \qquad (k= u, l) \qquad (2)$$

are the membrane, bending and shear strains respectively and the superscript "0" denotes the mid-plane of plate or shell element. For an orthotropic, linear elastic material, the sub-matrices in the material matrix are given by

$$A^k = \begin{bmatrix} A_{11}^k & A_{12}^k & A_{16}^k \\ A_{12}^k & A_{22}^k & A_{26}^k \\ A_{16}^k & A_{26}^k & A_{66}^k \end{bmatrix}, \qquad B^k = \begin{bmatrix} B_{11}^k & B_{12}^k & B_{16}^k \\ B_{12}^k & B_{22}^k & B_{26}^k \\ B_{16}^k & B_{26}^k & B_{66}^k \end{bmatrix}, \qquad (k= u, l) \tag{3a}$$

$$D^k = \begin{bmatrix} D_{11}^k & D_{12}^k & D_{16}^k \\ D_{12}^k & D_{22}^k & D_{26}^k \\ D_{16}^k & D_{26}^k & D_{66}^k \end{bmatrix}, \qquad H^k = \begin{bmatrix} H_{44}^k & H_{45}^k \\ H_{45}^k & H_{55}^k \end{bmatrix} \qquad (k= u, l) \tag{3b}$$

where

$$\begin{aligned} (A_{ij}^k,\ B_{ij}^k,\ D_{ij}^k) &= \int_{-h_k/2}^{h_k/2} \overline{Q}_{ij}^k (1,\ z,\ z^2)\mathrm{dz} \qquad (i, j = 1,\ 2,\ 6) \\ H_{ij}^k &= \frac{5}{4}\int_{-h_k/2}^{h_k/2} \overline{Q}_{ij}^k [1 - \frac{4z^2}{h_k^2}]\mathrm{dz} \qquad (i, j = 4,\ 5) \end{aligned} \qquad (k= u, l) \tag{4}$$

in which $\overline{Q}_{ij}^k$ is off-axis modulus, h_k (k=u, l) is the thickness of the upper and lower shell elements.

(b) Strain energy in the adhesive layer U_A

Basing on the assumptions given in the previous section, the strain energy in an adhesive layer is due to contributions of the three out-of-plane strains and can be written as

$$\begin{aligned} U_A &= \frac{1}{2}\int_{\text{Element area}} \{\varepsilon^A \quad \gamma_{yz}^A \quad \gamma_{xz}^A\}[D_A]\begin{Bmatrix} \varepsilon^A \\ \gamma_{yz}^A \\ \gamma_{xz}^A \end{Bmatrix} t dA \\ &= \frac{1}{2}\int_{\text{Element area}} \{\varepsilon^A \quad \gamma_{yz}^A \quad \gamma_{xz}^A\}\begin{bmatrix} E_A & 0 & 0 \\ 0 & G_A & 0 \\ 0 & 0 & G_A \end{bmatrix}\begin{Bmatrix} \varepsilon^A \\ \gamma_{yz}^A \\ \gamma_{xz}^A \end{Bmatrix} t dA \end{aligned} \tag{5}$$

where E_A and G_A are the equivalent normal and shear moduli of the adhesive layer. ε^A, γ^A_{xz} and γ^A_{yz} are the peel (normal) strain and the two shear strains, t is the adhesive thickness.

3.3. Element stiffness matrix

3.3.1. Element stiffness matrix for shell elements

For the two shell elements, the element stiffness matrix can be expressed as

$$[\mathbf{K}^k] = \int_{\text{Element area}} [B^k]^T [D^k][B^k] dA \qquad (k=u, l) \tag{6}$$

in which $[B^k] = \begin{bmatrix} B^k_m & B^k_b & B^k_s \end{bmatrix}$ and B^k_m, B^k_b and B^k_s are the matrix relating nodal displacement vector to strain vector for the element, e.g.,

$$\varepsilon^k_m = \begin{Bmatrix} \varepsilon^{0k}_{xx} \\ \varepsilon^{0k}_{yy} \\ \gamma^{0k}_{xy} \end{Bmatrix} = [B^k_m]\{q^k\}, \qquad \varepsilon^k_b = \begin{Bmatrix} k^{0k}_{xx} \\ k^{0k}_{yy} \\ k^{0k}_{xy} \end{Bmatrix} = [B^k_b]\{q^k\}$$

$$\varepsilon^k_s = \begin{Bmatrix} \gamma^k_{yz} \\ \gamma^k_{xz} \end{Bmatrix} = [B^k_s]\{q^k\} \qquad (k=u, l) \tag{7}$$

where $\{q^k\}$ $(k=u, l)$ denotes the nodal displacement vector of the thin-walled structure or the patch element.

3.3.2. Element stiffness matrix for the pseudo brick element

For the pseudo-brick element modeling the adhesive layer between the two shell elements, the peel and shear strains are assumed to be constant in the adhesive layer along the line between a pair of nodes. To illustrate the definition of the peel and two shear strains, let us consider a pair of nodes as shown in Figure 3-2, which are isolated from an adhesive element. According to the definition of the displacements of a degenerated plate or shell element, the nodal displacement of the pseudo-brick element modeling adhesive at the pseudo-node i' and j', can be expressed as

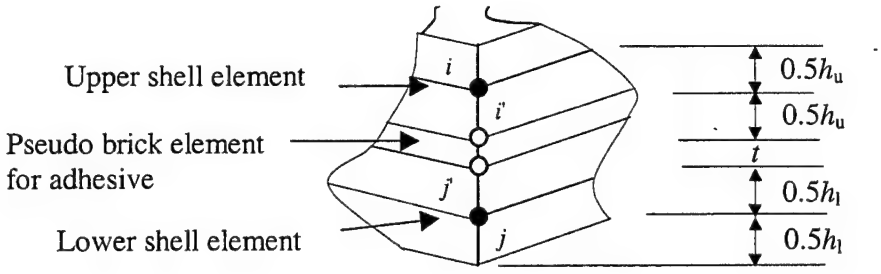

Figure 3-2 Schematic of a node pair

$$\begin{Bmatrix} u_{i'} \\ v_{i'} \\ w_{i'} \end{Bmatrix} = \begin{bmatrix} 1 & 0 & 0 & 0 & \frac{-h_u}{2} \\ 0 & 1 & 0 & \frac{h_u}{2} & 0 \\ 0 & 0 & 1 & 0 & 0 \end{bmatrix} \begin{Bmatrix} u_i^0 \\ v_i^0 \\ w_i \\ \theta_{xi} \\ \theta_{yi} \end{Bmatrix} \tag{8a}$$

$$\begin{Bmatrix} u_{j'} \\ v_{j'} \\ w_{j'} \end{Bmatrix} = \begin{bmatrix} 1 & 0 & 0 & 0 & \frac{h_l}{2} \\ 0 & 1 & 0 & \frac{-h_l}{2} & 0 \\ 0 & 0 & 1 & 0 & 0 \end{bmatrix} \begin{Bmatrix} u_j^0 \\ v_j^0 \\ w_j \\ \theta_{xj} \\ \theta_{yj} \end{Bmatrix} \tag{8b}$$

where the superscript "0"denotes the mid-plane, subscripts i and j denote the upper and lower shell elements, respectively. h_u and h_l represent the thickness of upper and lower shell elements.

The peel and two shear strains in the adhesive between pseudo-node i' and j' are constant and can be expressed as follows:

$$\begin{aligned} \varepsilon_{zz}^A &= \frac{1}{t}(w_i - w_j) \\ \gamma_{yz}^A &= \frac{1}{t}(v_{i'} - v_{j'}) = \frac{1}{t}(v_i^0 - v_j^0 + \frac{h_u}{2}\theta_{xi} + \frac{h_l}{2}\theta_{xj}) \\ \gamma_{xz}^A &= \frac{1}{t}(u_{i'} - u_{j'}) = \frac{1}{t}(u_i^0 - u_j^0 - \frac{h_u}{2}\theta_{yi} - \frac{h_l}{2}\theta_{yj}) \end{aligned} \tag{9a}$$

or rewrite in matrix form as

$$\begin{Bmatrix} \varepsilon_{zz}^{A} \\ \gamma_{yz}^{A} \\ \gamma_{xz}^{A} \end{Bmatrix}_{i'-j'} = \frac{1}{t}\begin{bmatrix} 0 & 0 & 1 & 0 & 0 & 0 & 0 & -1 & 0 & 0 \\ 0 & 1 & 0 & \frac{h_u}{2} & 0 & 0 & -1 & 0 & \frac{h_l}{2} & 0 \\ 1 & 0 & 0 & 0 & -\frac{h_u}{2} & -1 & 0 & 0 & 0 & -\frac{h_l}{2} \end{bmatrix} \begin{Bmatrix} u_i^0 \\ v_i^0 \\ w_i \\ \theta_{xi} \\ \theta_{yi} \\ u_j^0 \\ v_j^0 \\ w_j \\ \theta_{xj} \\ \theta_{yj} \end{Bmatrix} \tag{9b}$$

Similar equations can be developed to express the peel and shear strains in terms of the nodal displacements at every pair of nodes. By employing the same interpolation functions as the displacement fields within each shell element, the peel and shear strain fields can be established within the pseudo-brick element for adhesive layer, and written in the following format:

$$\begin{Bmatrix} \varepsilon_{zz} \\ \gamma_{yz} \\ \gamma_{xz} \end{Bmatrix} = \begin{bmatrix} B_A^u & B_A^l \end{bmatrix} \begin{Bmatrix} q^u \\ q^l \end{Bmatrix} \tag{10}$$

where B_A^u and B_A^l are the matrices relating the strains to the nodal displacements of both upper and lower shell elements. It is worth noting that the strains may be calculated in the local coordinate system or even in nodal coordinate system depending on which shell element is selected to construct the adhesive element.

The element stiffness matrix of the pseudo brick element for the adhesive layer can be expressed as follows

$$\left[\mathbf{K}^A\right]^e = \int_{\text{Element area}} [T]^T \begin{bmatrix} (B_A^u)^T \\ (B_A^l)^T \end{bmatrix} [D_A] \begin{bmatrix} B_A^u & B_A^l \end{bmatrix} [T] dA \tag{11}$$

where $[T]$ can be either the transforming matrix between the local and nodal coordinate system or the one between the local and global coordinate system, depending on the shell element selected.

Equation (11) can be rewritten in the following split form

$$\begin{aligned}\left[\mathbf{K}^{A}\right]^{e} &= \begin{bmatrix} \mathbf{K}_{uu}^{A} & \mathbf{K}_{ul}^{A} \\ \mathbf{K}_{lu}^{A} & \mathbf{K}_{ll}^{A} \end{bmatrix} \\ &= \int_{\text{Element area}} [T]^{T} \begin{bmatrix} [B_A^u]^T [D_A][B_A^u] & [B_A^u]^T [D_A][B_A^l] \\ [B_A^l]^T [D_A][B_A^u] & [B_A^l]^T [D_A][B_A^l] \end{bmatrix} [T] dA \end{aligned} \tag{12}$$

This is the expression for the element stiffness matrix for the pseudo-brick element for the adhesive layer.

3.3.3. Element stiffness matrix for adhesive element

The element stiffness matrix for the adhesive element, consisting of two shell elements and one pseudo brick element, can eventually be obtained by assembling the stiffness matrices of the two shell elements and the stiffness matrix of the pseudo brick element, namely,

$$[\mathbf{K}]^{e} = \begin{bmatrix} \mathbf{K}_{uu}^{A} + \mathbf{K}^{u} & \mathbf{K}_{ul}^{A} \\ \mathbf{K}_{lu}^{A} & \mathbf{K}_{ll}^{A} + \mathbf{K}^{l} \end{bmatrix} \tag{13}$$

The load vectors for mechanical and thermal loading cab be obtained following the routine finite element analysis procedure.

4. DEVELOPMENT OF THREE ADHESIVE ELEMENTS

Based on the fundamental formulations described in Section 3, this section presents the formulations for three specific adhesive elements, i.e., 8-node, 16-node and 18-node adhesive elements. The 8-node adhesive element is formulated in conjunction with two 4-node shell elements, while the 16- and 18-node adhesive elements are developed in conjunction with two 8-node Serendipity and 9-node Lagrange degenerated shell elements. To present the formulation for each adhesive element in a clear and concise form, the relevant shell element will be presented first and then followed by the formulation of the adhesive element.

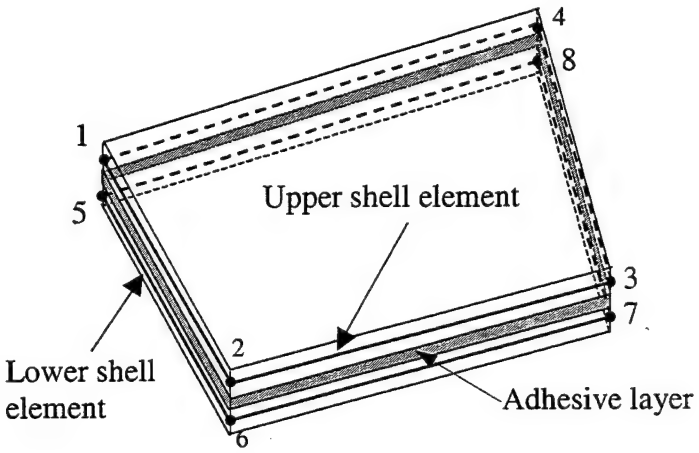

(a) Overall view

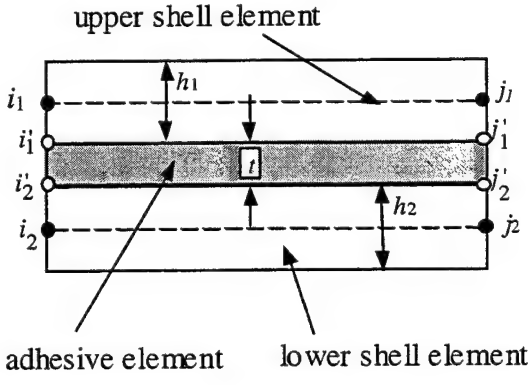

(b) Side view

Figure 4-1 Schematics views of the 8-node adhesive element in local coordinate system

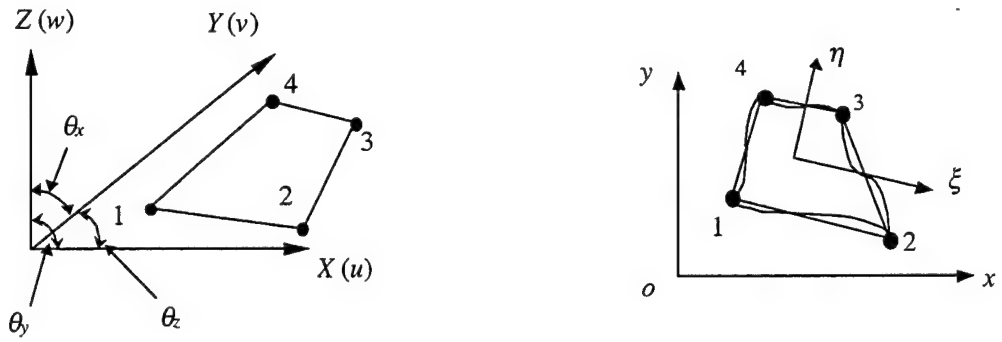

(a) global coordinate systems (b) local coordinate systems

Figure 4-2 The global and local coordinate systems

4.1. 8-Node adhesive element

Figure 4-1 depicts the 8-node adhesive element which consists of two 4-node shell elements and one pseudo brick element located in local coordinate system. In the figure, the mid-planes of the two shell elements are denoted by thicker lines, while the pseudo brick element is shaded for identification.

4.1.1. 4-node shell element

The 4-node shell element developed by Zhu and Zheng [7] is used to develop the 8-node adhesive element. In this 4-node shell element, the curved shell is approximately modeled using a 4-node flat plate element, in which an additional drilling degree of freedom is incorporated to enable simulation of all three translations and three rotations, i.e., the six degrees of freedom. The shell element is constructed in a flat plane in the local coordinate systems. Figure 4-2 depicts the coordinate systems used, e.g., the global coordinate system, the local coordinate system and the parametric plane coordinate system.

In the local coordinate system of the shell element, the first-order Reinssner-Mindlin plate theory is employed. The three displacements of the shell element in the local coordinate systems are defined as

$$U(x,y,z) = u^0(x,y) + z\theta_y(x,y)$$
$$V(x,y,z) = v^0(x,y) - z\theta_x(x,y) \qquad (14)$$
$$W(x,y,z) = w(x,y)$$

where u^0, v^0, w are the translational displacements in the mid-plane of the shell, and θ_x, θ_y are the rotations of the directional normal about x and y coordinate respectively. In the shell element, each node has 6 degrees of freedom, i.e., 3 translational degrees of freedom u^0, v^0, w and 3 rotational degrees of freedom θ_x, θ_y, θ_z. The displacement vector of the element can be written as:

$$\{q\}^e = (\{q_1\}^T \{q_2\}^T \{q_3\}^T \{q_4\}^T)^T \qquad (15)$$

where $\{q_i\}^T = (u_i^0 \quad v_i^0 \quad w_i \quad \theta_{x_i} \quad \theta_{yi} \quad \theta_{zi})$ (i =1,2,3,4). The displacement field in the shell element under the local co-ordinate systems can be divided into two parts

$$\{U\} = \{U^0\} + \{U_\theta\} \qquad (16)$$

The second term on the right hand side of the above is due to the rotation of the drilling degree of freedom. Both terms on the right hand side of equation (16) can be expressed in the form of the following interpolations

$$\{U^0\} = (u^0 \quad v^0 \quad w \quad \theta_x \quad \theta_y)^T = \sum_{i=1}^{4} N_i^0 (u_i^0 \quad v_i^0 \quad w_i \quad \theta_{xi} \quad \theta_{yi})^T \qquad (17a)$$

$$\{U_\theta\} = (u_\theta \quad v_\theta \quad 0 \quad 0 \quad 0)^T = \sum_{i=1}^{4} (N_{u_i} \quad N_{v_i} \quad 0 \quad 0 \quad 0)^T \theta_{z_i} \qquad (17b)$$

in which

$$N_i^o = (1+\zeta_i\zeta)(1+\eta_i\eta) \qquad (18a)$$

$$N_{u_1} = N_8\delta_{y_4} - N_5\delta_{y_1} \quad N_{u_2} = N_5\delta_{y_1} - N_6\delta_{y_2}$$
$$N_{u_3} = N_6\delta_{y_2} - N_7\delta_{y_3} \quad N_{u_4} = N_7\delta_{y_3} - N_8\delta_{y}$$
$$N_{v_1} = N_5\delta_{x_1} - N_8\delta_{x_4} \quad N_{v_2} = N_6\delta_{x_2} - N_5\delta_{x_1} \tag{18b}$$
$$N_{v_3} = N_7\delta_{x_3} - N_6\delta_{x_2} \quad N_{v_4} = N_8\delta_{x_4} - N_7\delta_{x_3}$$

and

$$N_5 = (1-\zeta^2)(1-\eta)/16 \quad N_6 = (1+\zeta)(1-\eta^2)/16$$
$$N_7 = (1-\zeta^2)(1+\eta)/16 \quad N_8 = (1-\zeta)(1-\eta^2)/16 \tag{19a}$$

$$\delta_{x_i} = x_j - x_i, \qquad \delta_{y_i} = y_j - y_i \quad j = (i \mod 4)+1 \tag{19b}$$

The displacement field in the element, therefore, can be written as follows

$$\{U\} = \{N_1 \quad N_2 \quad N_3 \quad N_4\}\{q\}^e \tag{20}$$

where

$$[N_i] = \begin{bmatrix} N_i^o & 0 & 0 & 0 & 0 & N_{u_i} \\ 0 & N_i^o & 0 & 0 & 0 & N_{v_i} \\ 0 & 0 & N_i^o & 0 & 0 & 0 \\ 0 & 0 & 0 & N_i^o & 0 & 0 \\ 0 & 0 & 0 & 0 & N_i^o & 0 \end{bmatrix} \quad (i=1,2,3,4) \tag{21}$$

It is well known that shear locking can take place for the element based on the Reinssner-Mindlin plate theory. This is due to inadequate match of the orders of interpolation functions used for both translational and rotational deformations. There are several schemes that can be used to remove shear locking, such as the reduced or selective integration, or assumed strain method [8]. In this element the assumed strain method is used to establish a novel set of shape functions to calculate the shear strains. In the parametric plane of ξ and η, the conventional bilinear shape functions for the two rotations with respect to the local parametric axes are replaced by the following single linear shape functions

$$\theta_\xi = a_0 + a_1\eta = \sum_{i=1}^{4} N_{\xi i}\theta_{\xi i}, \qquad \theta_\eta = b_0 + b_1\xi = \sum_{i=1}^{4} N_{\eta i}\theta_{\eta i} \tag{22}$$

The 8 single linear shape functions in the above equations can be determined by enforcing the following conditions:

$$\int_{-1}^{1}\int_{-1}^{1}(N_{\xi i}-N_i^0)^2\,d\xi d\eta=0, \qquad \int_{-1}^{1}\int_{-1}^{1}(N_{\eta i}-N_i^0)^2\,d\xi d\eta=0 \tag{23}$$

The eight new linear shape functions for the two rotations are then given by

$$N_{\xi i}=\frac{1}{4}(1-\eta_i\eta), \qquad N_{\eta i}=\frac{1}{4}(1-\xi_i\xi) \qquad (i=1,2,3,4) \tag{24}$$

The new interpolation functions for the two rotational deformations in equation (22) are used to calculate the two shear strain components, ε_{zx} and ε_{zy}, which are only employed in the formulation of the out-of-plane shear strain energy. It is worth pointing out that the original shape functions in equation (17a) and (18a) are still used in determination of the bending strain energy.

The strain energy term related to membrane and bending deformations can be determined using equations (17)-(19), and the shear strain energy terms can be calculated using equations (22) and (24). The stiffness matrix of the 4-node element can then be given by

$$[\mathbf{K}]=\int_{-1}^{1}\int_{-1}^{1}[T]^T[B]^T[D][B][T]\,|J|\,d\xi d\eta \tag{25}$$

where $[T]$ is the transformation matrix between the local and global coordinate systems, $[D]$ is the material property matrix of the shell element as defined in equations (3) and (4), and h is the thickness of the shell element. According to the relationship of strain-displacement in the shell element, matrix $[B]$ can be defined as

$$[B]=[B_1 \quad B_2 \quad B_3 \quad B_4] \tag{26}$$

in which

$$[B_i]=\begin{bmatrix} N^{o}_{i,x} & 0 & 0 & 0 & 0 & N_{u_{i,x}} \\ 0 & N^{o}_{i,y} & 0 & 0 & 0 & N_{v_{i,y}} \\ N^{0}_{i,y} & N^{0}_{i,x} & 0 & 0 & 0 & (N_{u_{i,y}}+N_{v_{i,x}}) \\ 0 & 0 & 0 & 0 & N^{0}_{i,x} & 0 \\ 0 & 0 & 0 & -N^{0}_{i,y} & 0 & 0 \\ 0 & 0 & 0 & -N^{0}_{i,x} & N^{0}_{i,y} & 0 \\ 0 & 0 & N^{0}_{i,y} & N_i^{yy} & N_i^{yx} & 0 \\ 0 & 0 & N^{0}_{i,x} & N_i^{xy} & N_i^{xx} & 0 \end{bmatrix} \tag{27}$$

where

$$\begin{aligned} N_i^{xx} &= -[N_{\xi i}(a_{12})_i b_{11} - N_{\eta i}(a_{22})_i b_{22}], \quad N_i^{xy} = N_{\xi i}(a_{11})_i b_{11} + N_{\eta i}(a_{21})_i b_{12} \\ N_i^{yx} &= -[N_{\xi i}(a_{12})_i b_{21} - N_{\eta i}(a_{22})_i b_{22}], \quad N_i^{yy} = N_{\xi i}(a_{11})_i b_{21} + N_{\eta i}(a_{21})_i b_{12} \end{aligned} \tag{28}$$

The terms a_{ij} and b_{ij} are the components in the Jacobian matrix $[J]$ between the local and parametric coordinate systems, and its inverse matrix $[J]^{-1}$, which is given by

$$[J]=\begin{bmatrix} a_{11} & a_{12} \\ a_{21} & a_{22} \end{bmatrix} \qquad [J]^{-1}=\begin{bmatrix} b_{11} & b_{12} \\ b_{21} & b_{22} \end{bmatrix} \tag{29}$$

It should pointed out that the terms given in equation (28), $(a_{ij})_i$, are the values of a_{ij} at node i of the shell element.

4.1.2. 8-node adhesive element

As shown in Figure 4-1(a) the adhesive element is represented by the shaded area which is sandwiched between the two four-node shell elements, i.e., element with nodes of 1 to 4, and element having nodes of 5 to 8. Figure 4-1(b) depicts a cross-sectional side view of the adhesive element in the local co-ordinate system. As shown in Figure 4-1(b), h_1, h_2 and h denote the thickness of the upper shell element, lower shell element and the adhesive element, respectively. i'_1, i'_2, j'_1 and j'_2 represent the pseudo nodes of the pseudo adhesive brick element between the two shell located at the adhesive-shell interfaces, i.e., the upper and lower surfaces of the adhesive layer related to the mid-plane node i_1, i_2, j_1 and j_2 of the

upper and lower shell elements. As shown in the figure, hollow circles show the pseudo nodes of the adhesive element, while the nodes of the shell elements are marked as solid circles.

Based on the assumptions in Section 3, the three displacements at pseudo node i'_1 and i'_2 of the adhesive element can be expressed in terms of nodal displacements of the upper and lower shell elements, as follows:

$$\begin{Bmatrix} u \\ v \\ w \end{Bmatrix}_{i'_1} = \begin{bmatrix} 1 & 0 & 0 & 0 & \frac{-h_1}{2} \\ 0 & 1 & 0 & \frac{h_1}{2} & 0 \\ 0 & 0 & 1 & 0 & 0 \end{bmatrix} \{\overline{q}_{i_1}\}$$

$$\begin{Bmatrix} u \\ v \\ w \end{Bmatrix}_{i'_2} = \begin{bmatrix} 1 & 0 & 0 & 0 & \frac{h_2}{2} \\ 0 & 1 & 0 & \frac{-h_2}{2} & 0 \\ 0 & 0 & 1 & 0 & 0 \end{bmatrix} \{\overline{q}_{i_2}\} \qquad (30)$$

where $\{\overline{q}_{i_1}\}^T = \{u^0_{i_1} + u_{\theta_1} \quad v^0_{i_1} + v_{\theta_1} \quad w^0 \quad \theta_{xi_1} \quad \theta_{yi_1}\}$ at node i_1 of the upper shell element and $\{\overline{q}_{i_2}\}^T = \{u^0_{i_2} + u_{\theta_2} \quad v^0_{i_2} + v_{\theta_2} \quad w^0 \quad \theta_{xi_2} \quad \theta_{yi_2}\}$ at node i_2 of the lower shell element.

Based on the assumptions, the three strain components in the local coordinates are constant along the line connecting node i'_1 and i'_2 in the adhesive element as shown in Figure 3(b) and can be expressed in terms of the corresponding nodal displacements of the upper and lower shell elements as follows:

$$\begin{Bmatrix} \varepsilon_{zz} \\ \gamma_{yz} \\ \gamma_{xz} \end{Bmatrix}_{i'_1 - i'_2} = \frac{1}{t} \begin{bmatrix} 0 & 0 & 1 & 0 & 0 & 0 & 0 & -1 & 0 & 0 \\ 0 & 1 & 0 & \frac{h_1}{2} & 0 & 0 & -1 & 0 & \frac{h_2}{2} & 0 \\ 1 & 0 & 0 & 0 & -\frac{h_1}{2} & -1 & 0 & 0 & 0 & -\frac{h_2}{2} \end{bmatrix} \begin{Bmatrix} \overline{q}_{i_1} \\ \overline{q}_{i_2} \end{Bmatrix} \qquad (31)$$

Substituting equations (17), (18) and (30) into equation (31) yields

$$\begin{Bmatrix} \varepsilon_{zz} \\ \gamma_{yz} \\ \gamma_{xz} \end{Bmatrix} = \begin{bmatrix} B_A^u & B_A^l \end{bmatrix} \begin{Bmatrix} q^u \\ q^l \end{Bmatrix} = \frac{1}{t} \begin{bmatrix} 0 & 0 & N_1^0 & 0 & 0 & 0 & \cdots \\ 0 & N_1^0 & 0 & \frac{h_1 N_1^0}{2} & 0 & N_{v1} & \cdots \\ N_1^0 & 0 & 0 & 0 & -\frac{h_1 N_1^0}{2} & N_{u1} & \cdots \end{bmatrix}$$

$$\begin{bmatrix} \cdots & 0 & 0 & -N_1^0 & 0 & 0 & 0 \\ \cdots & 0 & -N_1^0 & 0 & \frac{h_2 N_1^0}{2} & 0 & -N_{v1} \\ \cdots & -N_1^0 & 0 & 0 & 0 & -\frac{h_2 N_1^0}{2} & -N_{u1} \end{bmatrix} [T] \begin{Bmatrix} q_1 \\ q_2 \\ q_3 \\ q_4 \\ q_5 \\ q_6 \\ q_7 \\ q_8 \end{Bmatrix} \tag{32}$$

where q_i are defined in equation (15) and $[T]$ is the transforming matrix between the local and global system at element level. It is worth noting that the above formulation is applicable to the case when adhesive thickness is constant as assumed in Section 3. When the adhesive thickness varies, a modified formulation must be developed to replace the above equation and take into account the effect of variable adhesive thickness.

Substituting equation (32) into equation (11) and (12) yields the stiffness matrix of the pseudo brick element, which can be combined with the two stiffness matrices obtained using equation (25) to (27), to finally formulate an element stiffness matrix $[\mathbf{K}]_{48x48}$ as previously given in equation (13).

4.2. 16-Node adhesive element

Figure 4-3 depicts the 16-node adhesive element which consists of two 8-node Serendipity degenerated shell elements and one pseudo brick element. In the figure, solid circles denote the nodes of the two shell elements on the middle plane, while the hollow circles denote the pseudo nodes in the pseudo brick element as shaded for identification.

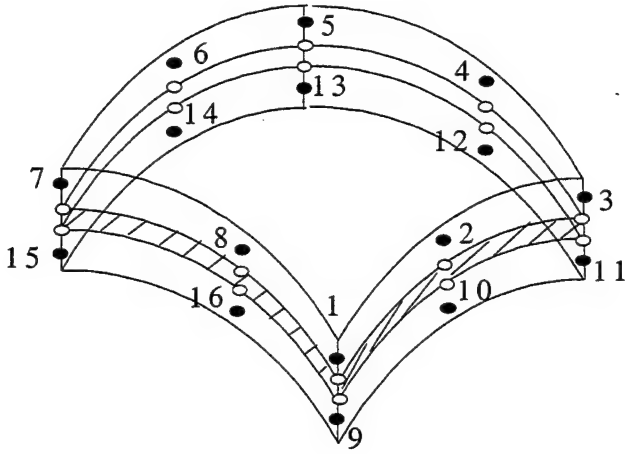

Figure 4-3 Configuration of the 16-node adhesive element

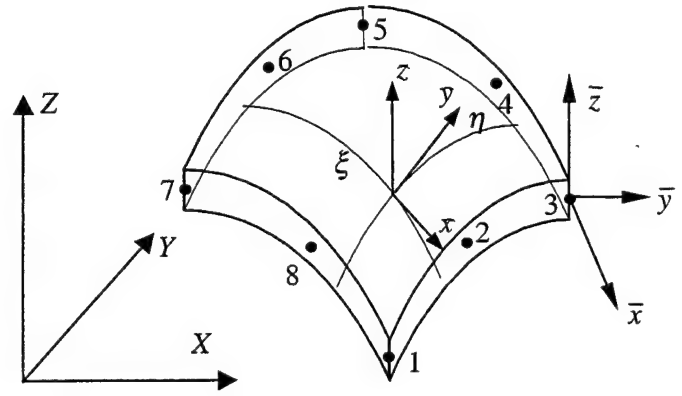

(a) Global, nodal and local co-ordinate system

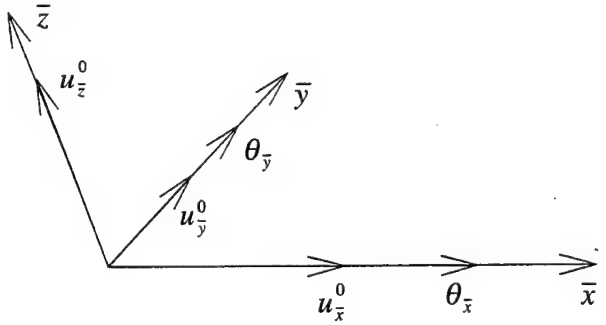

(b) Notation of nodal degrees of freedom

Figure 4-4 Global, nodal and local coordinate system and notation of nodal degrees of freedom

4.2.1. 8-node Serendipity shell element

Figure 4-4 depicts the shell element which is a curved lamina in three dimensional space. There are three Cartesian coordinate systems, namely, the global coordinate (X, Y, Z), the nodal coordinates ($\bar{x}$, $\bar{y}$, $\bar{z}$) and the local (or quadrature point) coordinates ($\hat{x}$, $\hat{y}$, $\hat{z}$). The shape functions are used to interpolate both the geometry of the mid-surface and displacement. Each node has 5 degrees of freedom; 3 translations ($u_{\bar{x}}^0$, $u_{\bar{y}}^0$, $u_{\bar{z}}^0$) and 2 rotations ($\theta_{\bar{x}}$, $\theta_{\bar{y}}$), as shown in Figure 4-4.

Every node of the structure is associated with a unique nodal system in which $\bar{z}$ is normal to the shell surface. The local systems ($\hat{x}$, $\hat{y}$, $\hat{z}$) are defined at each integration point with the $\hat{z}$ axis normal to the mid-plane and the $\hat{x}$, $\hat{y}$ axes in the tangent plane of the integration point. The global system is used as a reference for the other two systems.

The geometry of the degenerated shell is approximated by the isoparametric shape functions as follows:

$$\hat{x}_I = \sum_{i=1}^{8} N_i \hat{x}_{iI}^0 + \frac{h}{2}\zeta \sum_{i=1}^{8} N_i \hat{P}_{iI} \quad (I = 1,\ 2,\ 3) \tag{33}$$

where the expressions are written in the local co-ordinate system of a generic quadrature point. N_i is Serendipity isoparametric shape function. The superscript "0" denotes the quantities evaluated at the mid-plane of shell element. ζ is a coordinate along the normal of shell surface ranged (-1, 1) and h is the thickness of the shell. $\hat{P}_i$ is a unit vector pointing form the bottom node to the top node, which is defined by

$$\hat{p}_i = \frac{1}{h_i}(\hat{x}_i^{top} - \hat{x}_i^{bottom}) \tag{34}$$

The displacement field of the degenerated shell is governed by the constraint that the $\hat{\mathbf{P}}$ vectors remain straight in the deformed configuration, and is defined by

$$\hat{u}_I = \sum_{i=1}^{8} N_i \hat{u}_{il}^0 + \zeta \frac{h}{2} \sum_{i=1}^{8} N_i \begin{bmatrix} \hat{P}_{ix} & \hat{P}_{iy} \end{bmatrix} \begin{bmatrix} \hat{\theta}_x \\ \hat{\theta}_y \end{bmatrix} \tag{35}$$

Based on the classical shell theory, three kinds of strains can be given as

Membrane strains:

$$[\varepsilon_m] = \{B_{m1} \quad B_{m2} \quad \cdots \quad B_{m8}\} \begin{Bmatrix} q_1 \\ q_2 \\ \vdots \\ q_8 \end{Bmatrix} \tag{36a}$$

Bending strains:

$$[\varepsilon_b] = \{B_{b1} \quad B_{b2} \quad \cdots \quad B_{b8}\} \begin{Bmatrix} q_1 \\ q_2 \\ \vdots \\ q_8 \end{Bmatrix} \tag{36b}$$

Shear strains:

$$[\varepsilon_s] = \{B_{s1} \quad B_{s2} \quad \cdots \quad B_{s8}\} \begin{Bmatrix} q_1 \\ q_2 \\ \vdots \\ q_8 \end{Bmatrix} \tag{36c}$$

where

$$\{q_i\} = \{\hat{u}_i^0 \quad \hat{v}_i^0 \quad \hat{w}_i^0 \quad \hat{\theta}_{ix} \quad \hat{\vartheta}_{iy}\} \tag{36d}$$

$$[B_{mi}] = \begin{bmatrix} B_{i\tilde{x}}^0 & 0 & 0 & 0 & 0 \\ 0 & B_{i\tilde{y}}^0 & 0 & 0 & 0 \\ B_{i\tilde{y}}^0 & B_{i\tilde{x}}^0 & 0 & 0 & 0 \end{bmatrix}, \qquad [B_{bi}] = \begin{bmatrix} B_{i\tilde{x}}^1 & 0 & 0 & 0 & B_{\tilde{x}}^0 \\ 0^T & B_{i\tilde{y}}^1 & 0 & -B_{i\tilde{y}}^0 & 0 \\ B_{i\tilde{y}}^1 & B_{i\tilde{x}}^1 & 0 & -B_{i\tilde{x}}^0 & B_{i\tilde{y}}^0 \end{bmatrix},$$

$$[B_{si}]=\begin{bmatrix}0 & 0 & B^0_{i\tilde{x}} & 0 & N_i\\ 0 & 0 & B^0_{i\tilde{y}} & -N_i & 0\end{bmatrix} \tag{36e}$$

$$\begin{Bmatrix}B^0_{i\tilde{x}}\\ B^0_{i\tilde{y}}\end{Bmatrix}=\frac{1}{c_0}\begin{bmatrix}\hat{y}^0_{,\eta} & -\hat{y}^0_{,\xi}\\ -\hat{x}^0_{,\eta} & \hat{x}^0_{,\xi}\end{bmatrix} \qquad \begin{Bmatrix}B^1_{i\tilde{x}}\\ B^1_{i\tilde{y}}\end{Bmatrix}=\frac{1}{c_0}\begin{bmatrix}p_{\tilde{y},\eta}-c\hat{y}^0_{,\eta} & -(p_{\tilde{y},\xi}-c\hat{y}^0_{,\xi})\\ -(p_{\tilde{x},\eta}-c\hat{x}^0_{,\eta}) & p_{\tilde{x},\xi}-c\hat{x}^0_{,\xi}\end{bmatrix} \tag{36f}$$

$$\begin{aligned}c_0 &= \hat{x}^0_{,\xi}\hat{y}^0_{,\eta}-\hat{x}^0_{,\eta}\hat{y}^0_{,\xi}\\ c &= c_1/c_0\\ c_1 &= \hat{x}^0_{,\xi}p_{\tilde{y},\eta}+\hat{y}^0_{,\eta}p_{\tilde{x},\xi}-\hat{x}^0_{,\eta}p_{\tilde{y},\xi}-\hat{y}^0_{,\xi}p_{\tilde{x},\eta}\end{aligned} \tag{36g}$$

It be seen that the definition of bending strain in equation (36e) differs from that for resultant-stress degenerated shell element by the fact that the first two columns of B_b are not zero, the additional terms reflect the contributions of displacements to the curvature. The detailed derivation of (36) can be found in reference [9, 10].

All the strains in Equation (36) are evaluated in local coordinate system that is located at the Gauss integration point and the element stiffness matrices are also formed in this local coordinate system. Then the local element matrices must be transformed into the nodal system to assembly.

4.2.2. 16-node adhesive element

A 16-node adhesive element, which is located in the middle of two 8-node shell element, is shown in Figure 4-3. All the symbols are similar with those in Figure 4-1.

Followed by the same procedure as described in Section 4.1.2, three strains in the adhesive element can then be given by

$$\begin{Bmatrix}\hat{\varepsilon}_{zz}\\ \hat{\gamma}_{yz}\\ \hat{\gamma}_{xz}\end{Bmatrix}=\frac{1}{t}\begin{bmatrix}0 & 0 & N_1 & 0 & 0 & \cdots & 0 & 0 & -N_1 & 0 & 0 & \cdots\\ 0 & N_1 & 0 & \frac{h_1N_1}{2} & 0 & \cdots & 0 & -N_1 & 0 & \frac{h_2N_1}{2} & 0 & \cdots\\ N_1 & 0 & 0 & 0 & -\frac{h_1N_1}{2} & \cdots & -N_1 & 0 & 0 & 0 & -\frac{h_2N_1}{2} & \cdots\end{bmatrix}[T]_p\begin{Bmatrix}q_1\\ q_2\\ \vdots\\ q_{16}\end{Bmatrix}$$
$$=[B][T]_p\{q\} \tag{39}$$

where $\{q_i\}$ is defined in equation (36d) and $[T]_p$ is the transforming matrix between the local and nodal co-ordinate system at nodal level. All the strains are evaluated in the local co-ordinate system and adhesive element stiffness matrix must be transformed into the nodal coordinate system before it is assembled to the total stiffness matrix.

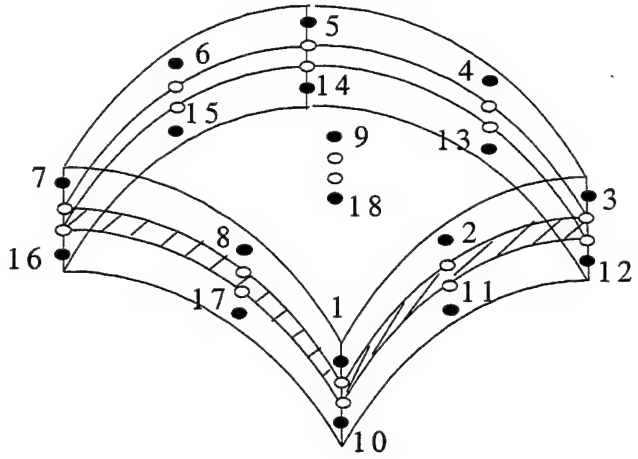

Figure 4-5 Configuration of the 18-node adhesive shell element

4.3. 18-node adhesive element

Figure 4-5 depicts the 18-node adhesive element which consists of two 9-node Lagrange degenerated shell elements and one pseudo brick element. All the symbols and marks are the same as those in Figure 4-3.

The 9-node Lagrange degenerated shell elements is constructed by the same method as described in Section 4.2. The difference between 9-node and 8-node shell element is that different interpolation shape functions are used. An assumed strain stabilization procedure is introduced into 9-node shell element to avoid any spurious singular modes. For further derivation, please see reference [9, 10].

All the formulations for 18-node adhesive element can be obtained in a same way as that for 16-node adhesive element.

5. Numerical Verification

To validate the developed adhesive elements, this section compares the stresses in adhesive layer predicted using the present software called BPATCH with those obtained using commercially available finite element analysis software STRAND 7.

Let us consider a cantilever curved beam with a bonded patch as depicted in Figure 5.1. It is assumed that the patch is perfectly bonded to the parent beam. Both the beam and patch have the same thickness of H=1 mm. The parent beam has a radius of curvature of R=100 mm. The bondline thickness is t=0.15 mm. The arc length of the patch is only half of that of the parent beam, which has a sector angle of 30°. Both the parent beam and reinforcing patch are clamped at the left end of θ=0°, and free at the other end. A vertical load of 20 N/mm is uniformly distributed along the width direction of the beam and applied on the middle plane of the parent beam at the free end, as shown in Figure 5-1. The width of the parent beam and patch is 10 mm.

Both the parent beam and patch are assumed to be aluminum with a Young's modulus of E=70GPa and a Poisson's ratio of v=0.3. The adhesive has a Young's modulus of Ec=2.4GPa and a Poisson's ratio of v_c=0.33.

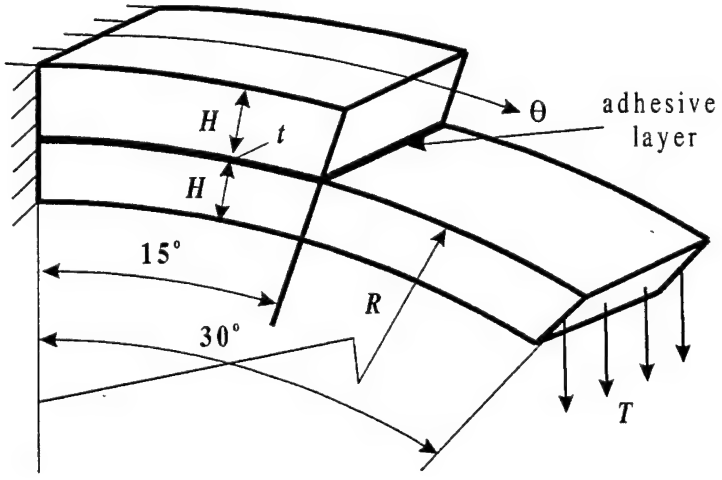

Figure 5-1 Cantilever curved beam under vertical load

A commercial finite element analysis software called STRAND 7 is used to analyze the problem and to serve as a benchmark for the new software BPATCH. Brick elements are

used to model the beam, patch and the adhesive layer. A large number of brick elements are used to maintain an appropriate aspect ratio of close to square elements in the R-θ plane near the end of the adhesive layer, namely, one brick element across the adhesive layer. Fine mesh of brick size of 0.15 mm is used near adhesive end and coarse mesh is used in the rest part of the structure. The arc length of the overlap is modeled using 30 by 2 newly developed adhesive elements, and the unsupported part is modeled with 15 by 2 corresponding shell elements using the BPATCH software to calculate the stresses in the adhesive layer.

Figures 5-2 and 5-3 show the distributions of the shear stress σ_{RT} and peel stress σ_{RR} in the adhesive layer, which are calculated by utilizing different adhesive elements and STRAND7. It can be seen that the predictions given by the present three adhesive elements correlate well with the results of STRAND7. It should be noted that the size of element near the right end of the adhesive layer is only suitable for engineering purpose as it does allow that the shear stress becomes zero at the end of the squared-edged adhesive layer. It is noted that slight oscillations in shear stress predicted using the 16-node element and peel stress predicted using the 8-node element are observed at low stress level. This may be due to existence of spurious zero energy modes.

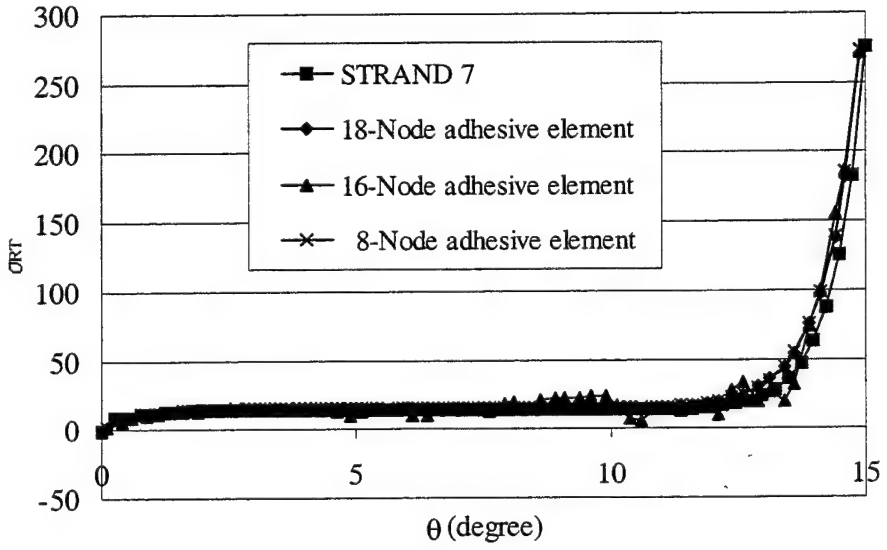

Figure 5-3 Shear stress distribution along the circumferential direction θ varying from 0 to 15°

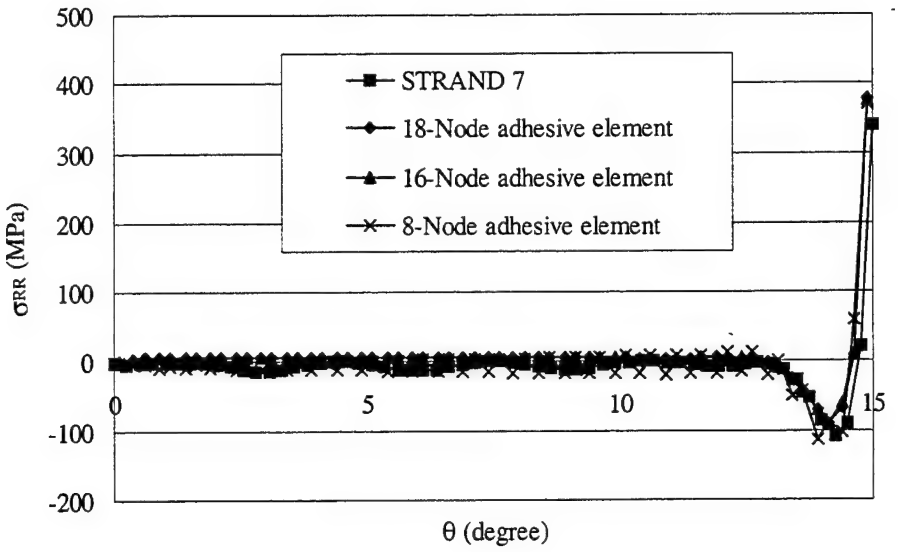

Figure 5-3 Peel stress distribution along the circumferential direction θ varying from 0 to 15°

6. Numerical Results and Discussion

In the section, some numerical results are obtained using the new software BPATCH to investigate the effect of curvature on stresses in adhesive layer for a number of combinations of geometrical configurations, boundary and loading conditions;

6.1. Single curved lap joint subjected to tensile load

Figure 6-1 depicts a curved single-lap type of joint between two circular cylindrical shells under tensile loading at both ends. The joint is assumed to be simply supported at the both ends of the unsupported shell. The horizontal distance between both ends and the middle point of the overlap is l=150mm. The half arc length of the bonded overlap is c=30mm. The width of joint is w=10mm. Both shells have the same thickness of H=5.0mm. The adhesive layer has a nominal thickness of t=0.15mm. The applied load at both ends is T=60N/mm, which is uniformly distributed along the width direction. Both shells have the same Young's modulus of E=70GPa and Poisson's ratio of ν=0.3. The adhesive has a Young's modulus of E_c=2.4GPa and a Poisson's ratio of ν_c=0.33.

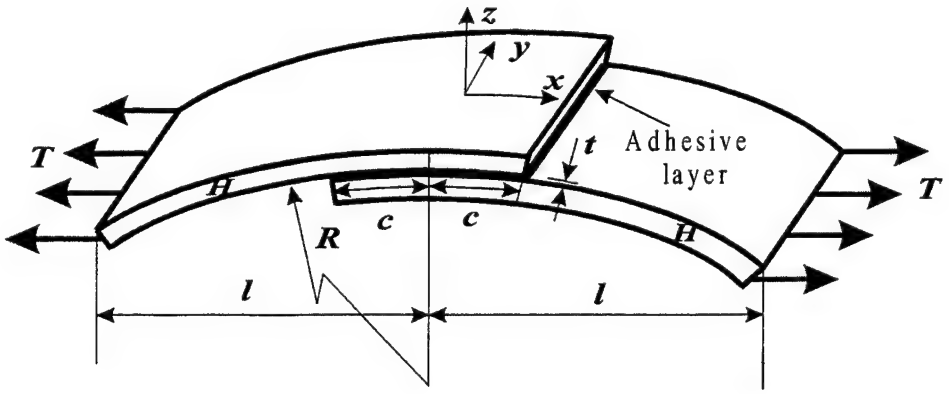

Figure 6-1 Schematic of a curved single-lap joint under tensile loading

Figures 6-2 and 6-3 plot the peel stress σ_{zz} and the shear stress σ_{zx} in the adhesive layer of the curved single-lap joints along the full arc length x ranging from $-c$ to c. In the figure, four values of the radius of curvature are selected, and they are R=2500, 5000, 10000 and infinity. Apparently when R=infinity, the joint becomes the classical flat single-lap joint. The results for R=infinity correlates well with the classical solution [5,6]. The two figures also show that, at the right end of the overlap, the peak peel stress varies from a positive value to a

negative one and the peak shear stress changes from a negative value to a positive one when the curvature (1/R) is increased from zero to 1/2500. The peak peel and shear stresses at the left end increase significantly in their absolute values but remain unchanged in their sign when the joint varies from a flat one to a curved one with a larger curvature. It is clear that a curved joint has a higher positive peak peel stress and larger shear stress than a flat one. As the peak peel stress is deem as the major contributing factor to peel dominant failure, it is believed that a curved single-lap joints is not preferred, and a flat single-lap joint carries more load than a curved single-lap one does.

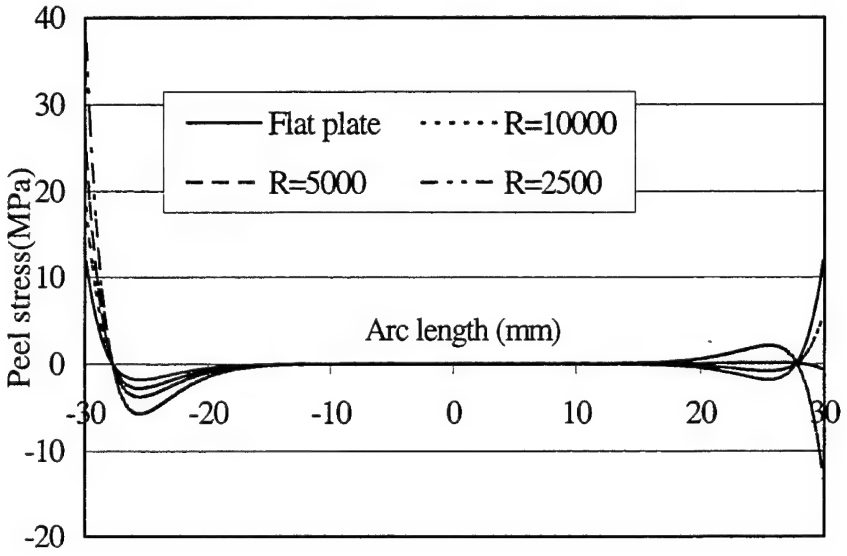

Figure 6-2 Comparison of peel stress distribution for the curved single-lap joints with various values of radius of curvature

Figure 6-4 plots the peak peel and shear stresses at both ends versus the curvature for the single-lap joint considered. The solid and dashed lines denotes the results for peak peel and shear stresses respectively. It is clear that the absolute values of peak peel and shear stresses at the left end increase dramatically with an increased value of curvature. Same trends are also observed for the peak peel and shear stresses at the right end although there is a sign change when the curvature increases from zero to 10^{-4}. The significant effect of curvature on peak stresses in adhesive layer implies that a great care must be taken when designing bonded joints having curvatures. The solutions from flat joints may not be directly transformed to those for curved joints.

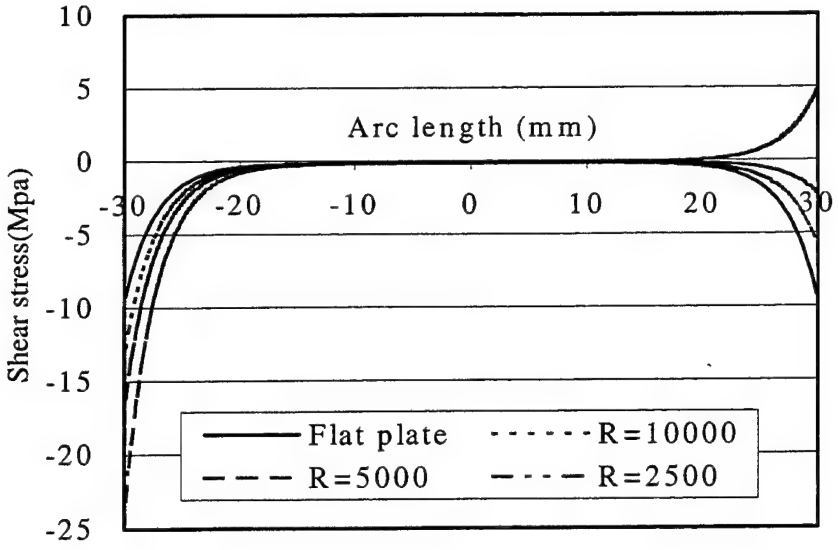

Figure 6-3 Comparison of shear stress distribution for the curved single-lap joints with various values of radius of curvature

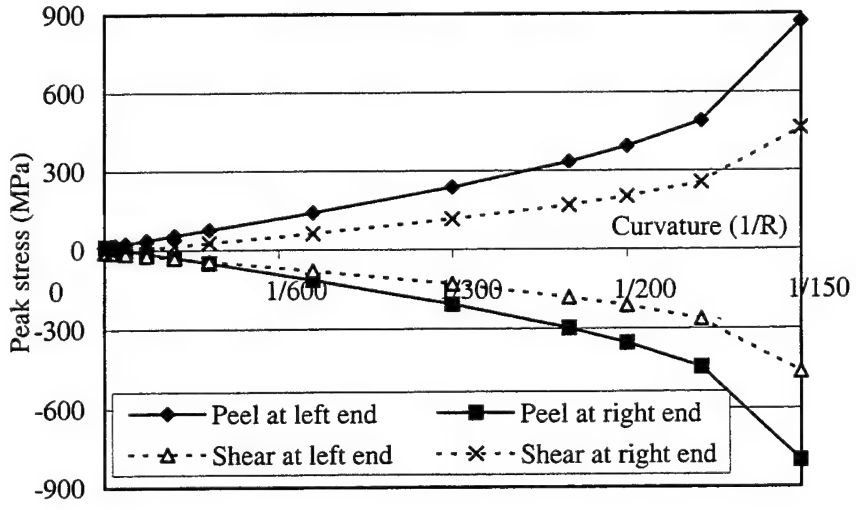

Figure 6-4 Peak stresses at both ends of the adhesive layer versus the curvature 1/R

6.2. A cylindrical shell bonded two external patches symmetrically

Figure 6-5 depicts a circular cylindrical shell bonded two external patches which are located symmetrically about the vertical line passing through the center of the shell. The longitudinal coordinate y is measured from the middle length of patch, which the circumferential coordinate x starts from one of the straight edges and is measured towards the other straight

edge. The length and width of the patch are the same and are equal to L=C=30mm. The overall length of the shell is W=300mm. The radius of the shell is R=150mm. The thickness of the cylindrical shell and the patches are all 5.0mm. The thickness of adhesive layer is t=0.15mm. The longitudinal and circumferential coordinate y and x vary from –15 to 15 and from 0 to 30, respectively.

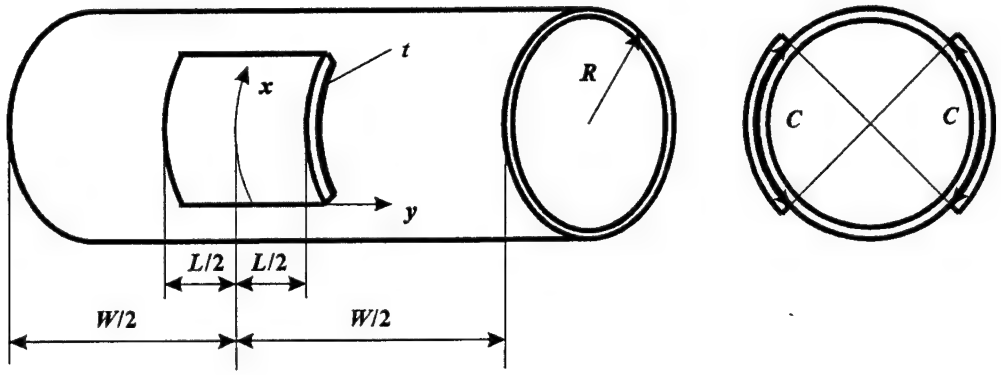

Figure 6-5 A cylinder bonded two external patches symmetrically

The shell is assumed to be metallic with a Young's modulus of E=70GPa and Poisson's ratio of ν=0.3. The adhesive used has a Young's modulus of E_c=2.4GPa and a Poisson's ratio of ν_c=0.33. To study the effect of different patching materials, two types of materials are used for the patches, one is metal with the same material properties as the shell itself, and the other is composite materials with all fibers aligned in the circumferential direction, i.e., in x-direction. The material properties adopted for a typical lamina are: $E_1 = 131.0GPa$, $E_2 = E_3$=11.2GPa, G_{12}=G_{13}=6.55GPa, G_{23}=4.375GPa and $\mu_{12} = \mu_{13}$=μ_{23}=0.28.

Both ends of the cylindrical shells are supported by rigid diaphragms, which allow displacements only in the axial direction of the shell. There are two types of loading cases, internal pressure and external pressure, considered. The applied pressure is p=1.0MPa.

Due to symmetry, only one quarter of the cylindrical shell is modeled using a finite element mesh with 15×15 elements used for the patch.

The BPATCH software is used to calculate the stresses in the adhesive layer for this problem, which has four combinations:

(a) metallic shell with metallic patches under internal pressure

(b) metallic shell with metallic patches under external pressure

(c) metallic shell with composite patches under internal pressure

(d) metallic shell with composite patches under external pressure

All four material and loading combinations are analyzed, however, due to space limitation only the results for the last two cases are presented in details.

Figures 6-6 to 6-8 and 6-9 to 6-11 show the distributions of stresses in the adhesive layer for the shell with two externally bonded composite patches subjected to internal and external pressure respectively. Figures 6-6 and 6-9 depict the three-dimensional distribution patterns of the three stresses, peel stress σ_{zz} and two shear stresses τ_{yz}, τ_{xz}, over half of the patch. Evidently, the peel stress σ_{zz} is symmetrical with respect to y=0 and x=15, the shear stress τ_{xz} is symmetrical with respect to y=0, and the shear stress τ_{yz} is anti-symmetrical about y=0. It is clearly seen that peak values of all stresses seem to take place near the corners of the patch, which implies that a shape optimization near the corner must be performed in order to achieve an optimum shape design of the corner areas. From these two figures, it is seen that the shear stress τ_{yz} is in general much smaller than other two stresses. The figures also reveal that high stresses occur along the y direction near one of the two straight edges of the patch, i.e., when x=0 or along the x direction near one of the two curved edges of the patch, i.e., when y is close to 15.

Figures 6-7 and 6-10 show the stress distributions of the three stress components along the longitudinal axis y at x=0, which represents one straight edge of the bonded patch and along which all three stresses tend to be more critical than others. Figures 6-8 and 6-11 depict the stress distributions along x-axis at the location of y where the corresponding stress reaches a peak near the curved edge of the patch. It is clearly seen that the peel stress along the straight edge for the case when subjected to an external pressure is much larger than that for the case when subjected to an internal pressure. As can be seen from Figures 6-8 and 6-11, at or near each corner the peel stress for the case under an external pressure is about 25 MPa comparing to 3 MPa for the case under internal pressure. This result indicates that it is preferred to apply an internal pressure to the shell with two external bonded composite patches rather than to apply an external pressure.

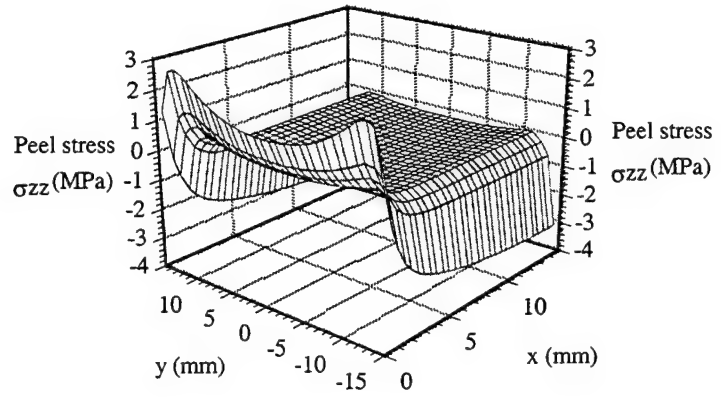

(a) Peel stress σ_{zz}

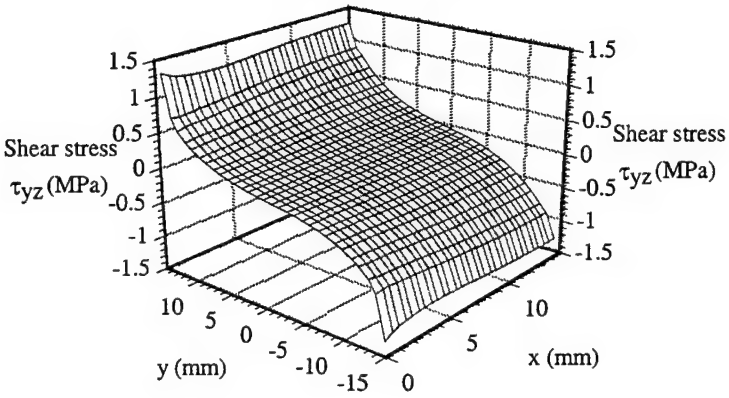

b) Shear stress τ_{yz}

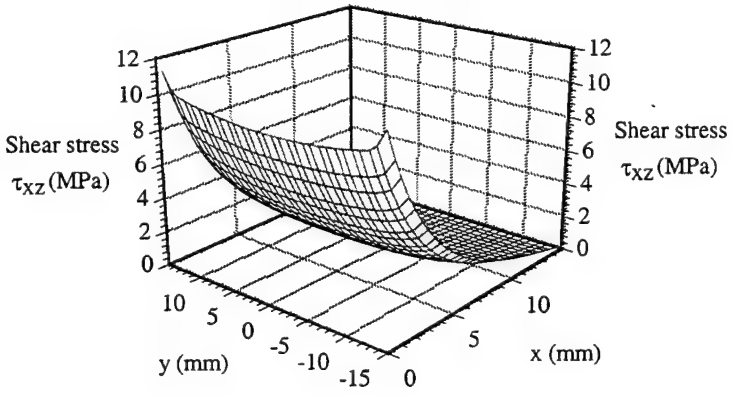

(c) Shear stress τ_{xz}

Figure 6-6 Stress distributions in the metallic cylindrical shell with two bonded external composite patches subjected to internal pressure

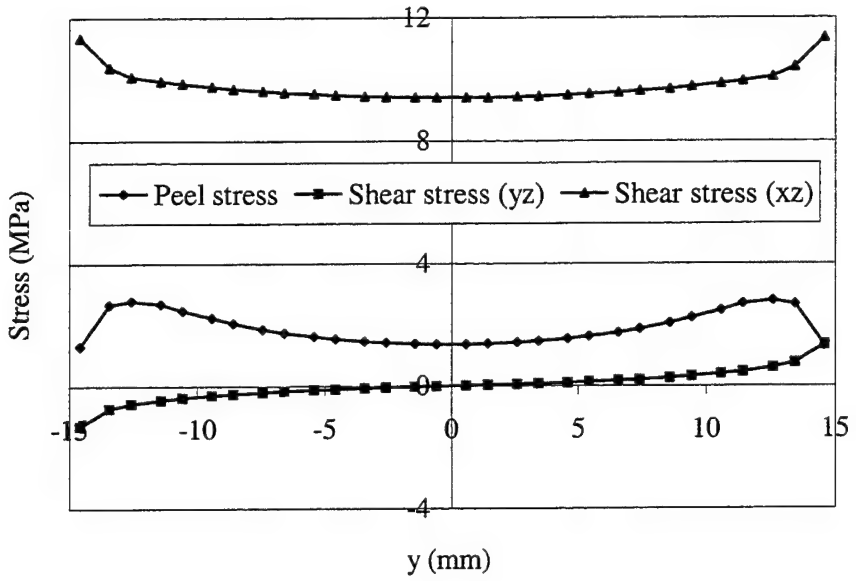

Figure 6-7 Stress distribution along y-axis at x=0 for the metallic cylindrical shell with two bonded external composite patches subjected to internal pressure

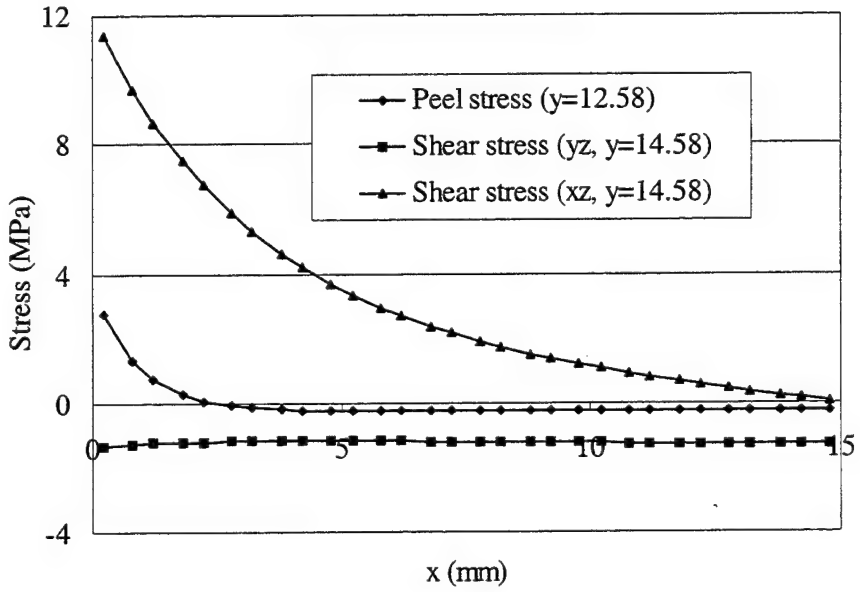

Figure 6-8 Stress distribution along x-axis with peak stress for the metallic cylindrical shell with two bonded external composite patches subjected to internal pressure

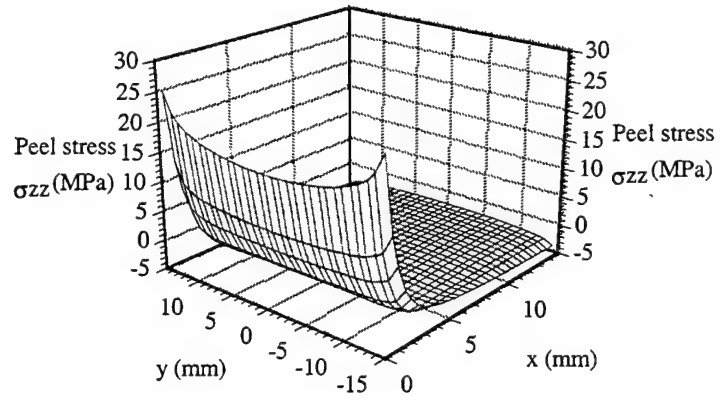

(a) Peel stress σ_{zz}

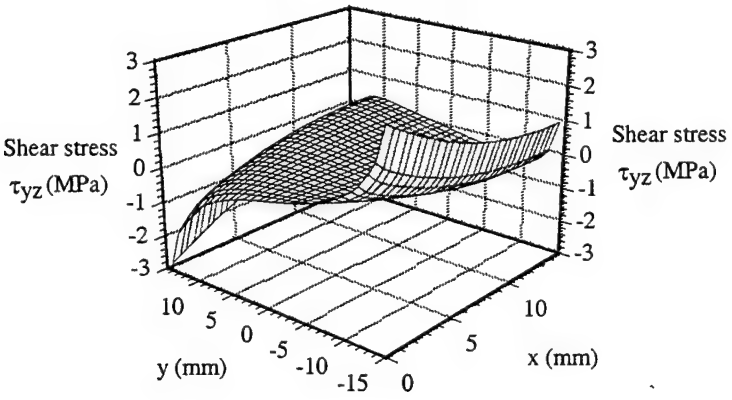

(b) Shear stress τ_{yz}

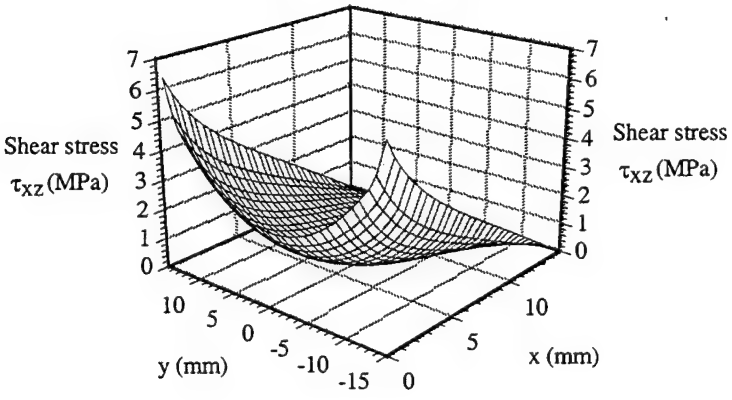

(c) Shear stress τ_{xz}

Figure 6-9 Stress distribution for the cylindrical shell with two bonded external composite patches subjected to external pressure

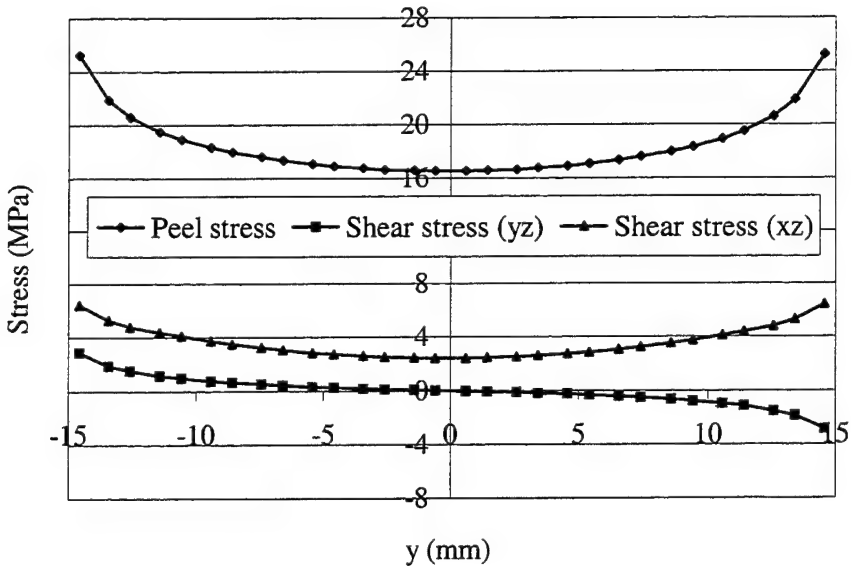

Figure 6-10 Stress distribution along y-axis at x=0 for the metallic cylindrical shell with two bonded external composite patches subjected to external pressure

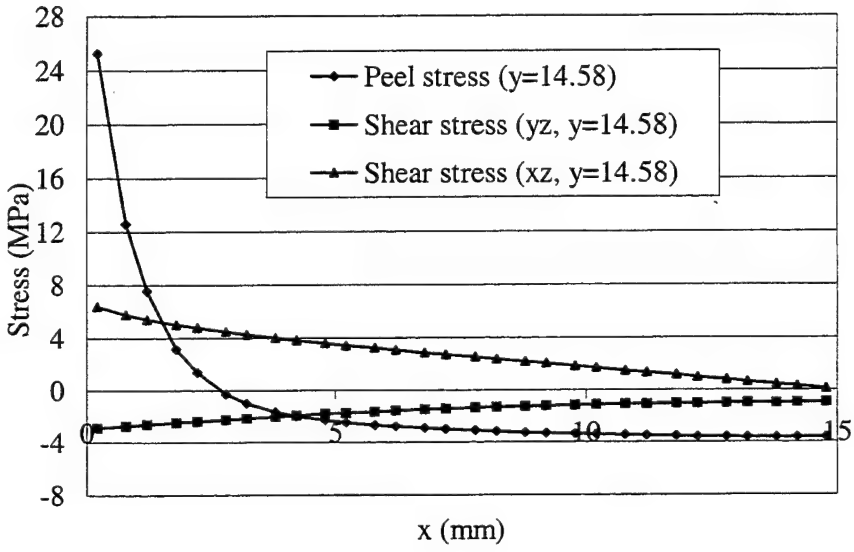

Figure 6-11 Stress distribution along x-axis with peak stress for the metallic cylindrical shell with two bonded external composite patches subjected to external pressure

6.3 A cylindrical shell bonded two internal patches symmetrically

This example is the same as that given in the previous section except that two externally bonded patches are replaced by two internally bonded patches. Figure 6-12 schematically depicts the shell with two internally bonded patches.

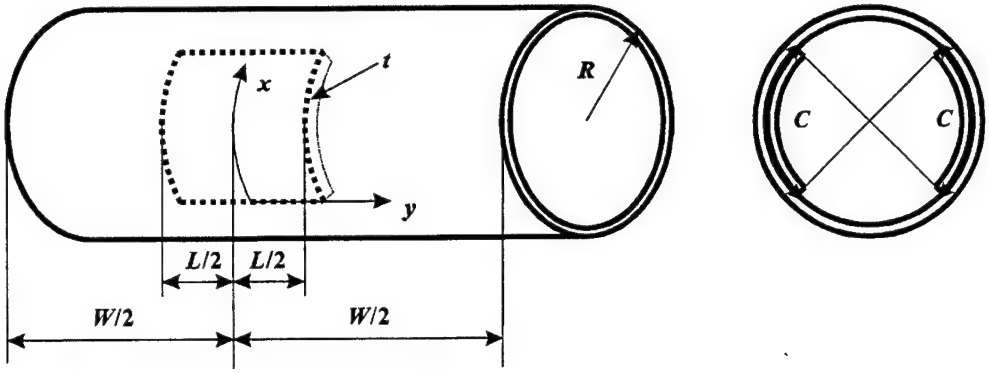

Figure 6-12 A cylinder bonded two internal patches symmetrically

All geometrical and material parameters and all boundary and loading conditions are the same as those used in Section 6.2.

Figures 6-13 to 6-15 and 6-16 to 6-18 show the distributions of stresses in the adhesive layer for the shell with two internally bonded composite patches subjected to internal and external pressure respectively. Figures 6-13 and 6-16 depict the three-dimensional distribution patterns of the three stresses over half of the patch. Similarly, peak stresses seem to take place near the corners of the patch. However, for the case under external pressure, the peak positive peel stress occurs along the mid-span of curved edge of the patch. Once again, it is seen that the shear stress τ_{yz} is in general smaller than other two stresses. It is clearly found that the peel stress along the straight edge for the case when subjected to an internal pressure is much larger than that for the case when subjected to an external pressure. As can be seen from the Figures, peak peel stress for the case under an internal pressure is just above 30 MPa comparing to about 2 MPa for the case under an external pressure. This result indicates that it is preferred to apply an external pressure to the shell with two internal composite patches rather than to apply an internal pressure.

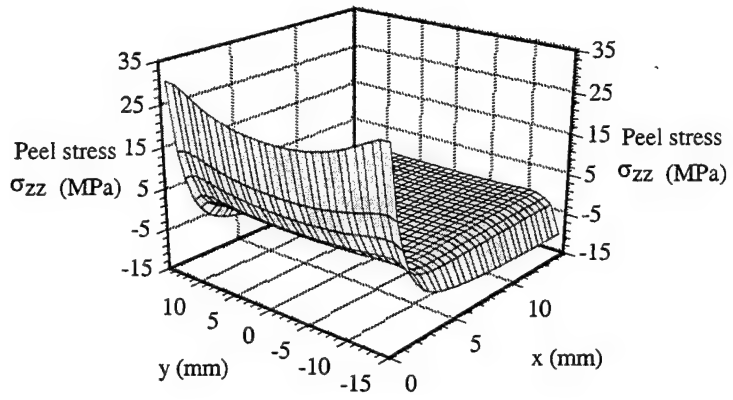

(a) Peel stress

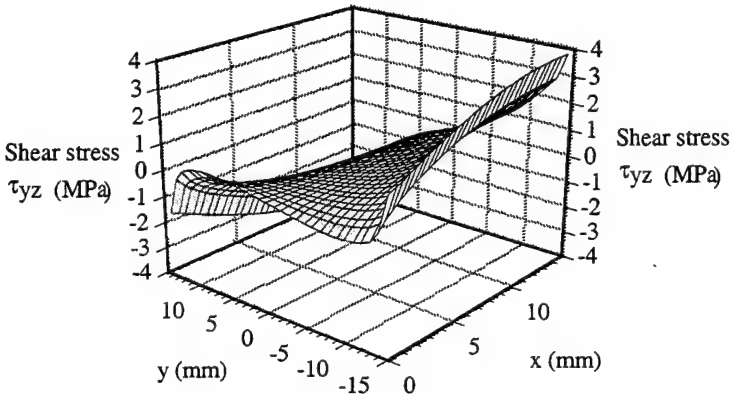

(b) Shear stress

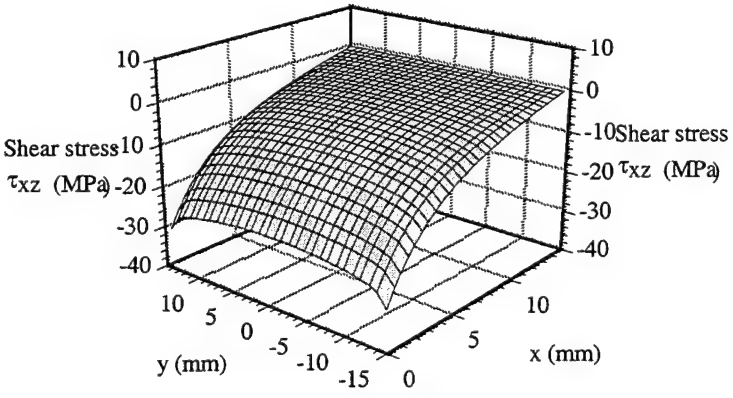

(c) Shear stress

Figure 6-13 Stress distribution for the metallic cylindrical shell bonded two internal composite patches subjected to internal pressure

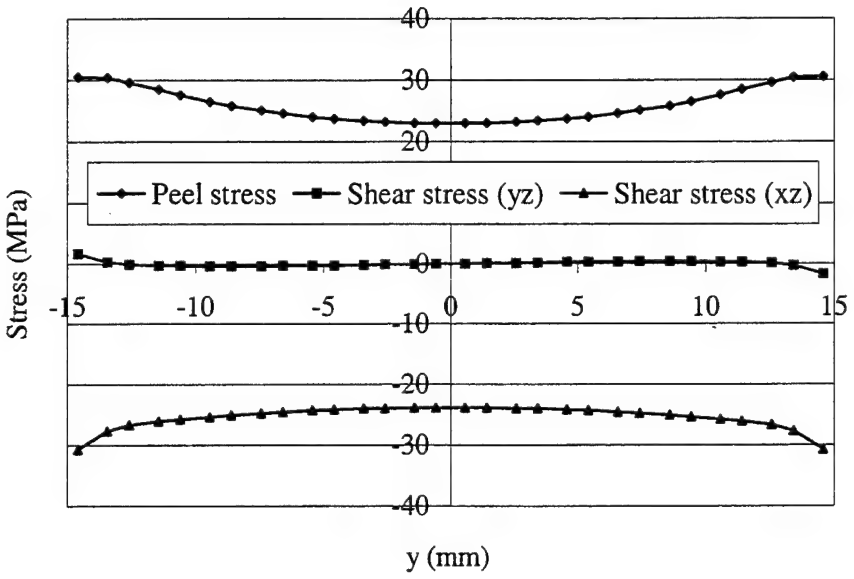

Figure 6-14 Stress distribution along y-axis at x=0 for the metallic cylindrical shell bonded two internal composite patches subjected to internal pressure

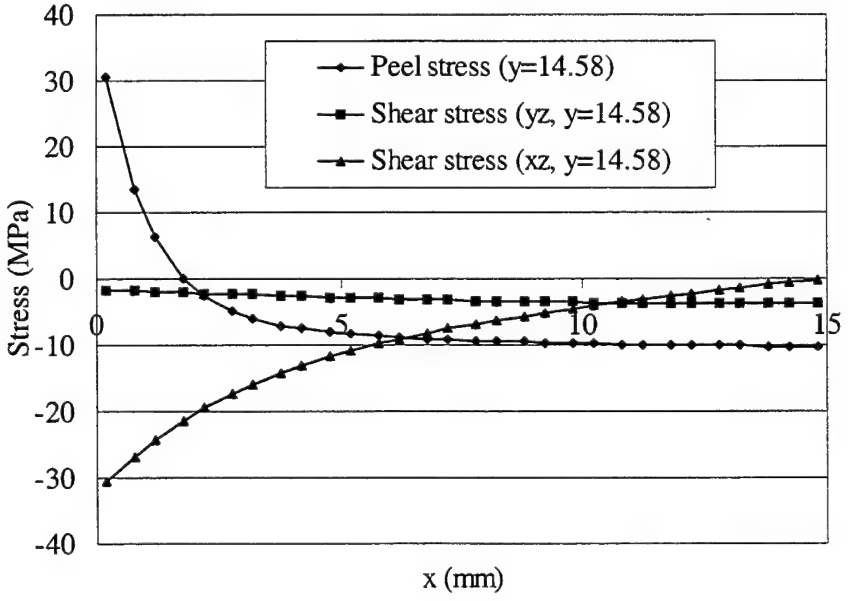

Figure 6-15 Stress distribution along x-axis with peak stress for the metallic cylindrical shell bonded two internal composite patches subjected to internal pressure

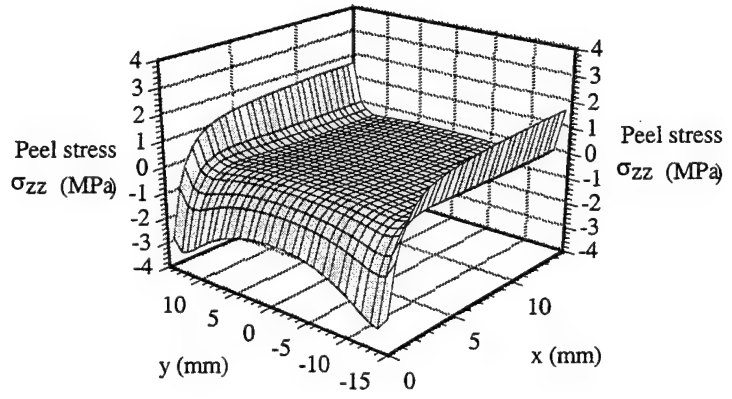

(a) Peel stress

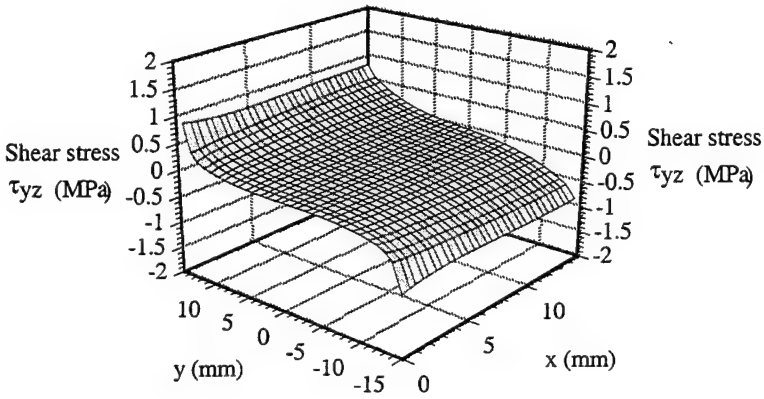

(b) Shear stress

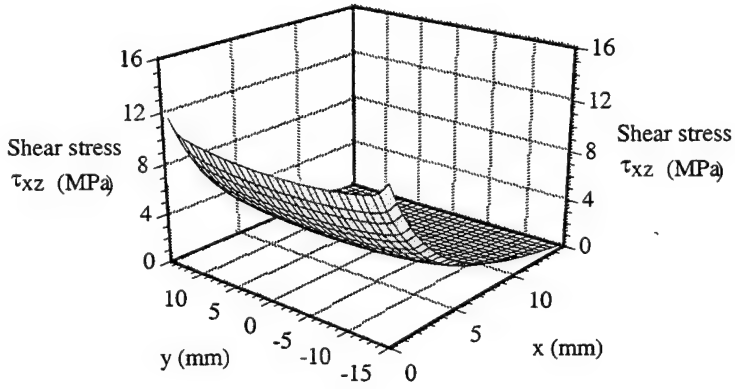

(c) Shear stress

Figure 6-16 Stress distribution for the metallic cylindrical shell bonded two internal composite patches subjected to external pressure

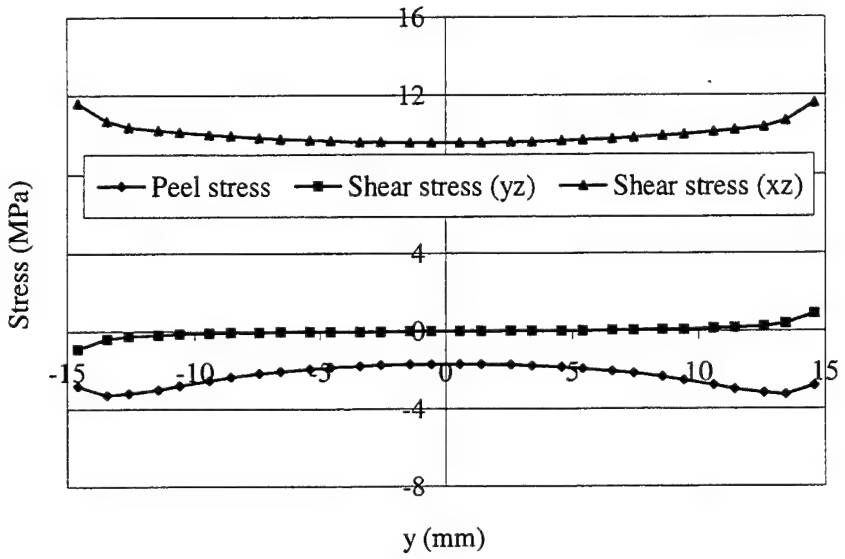

Figure 6-17 Stress distribution along y-axis at x=0 for the metallic cylindrical shell bonded two internal composite patches subjected to external pressure

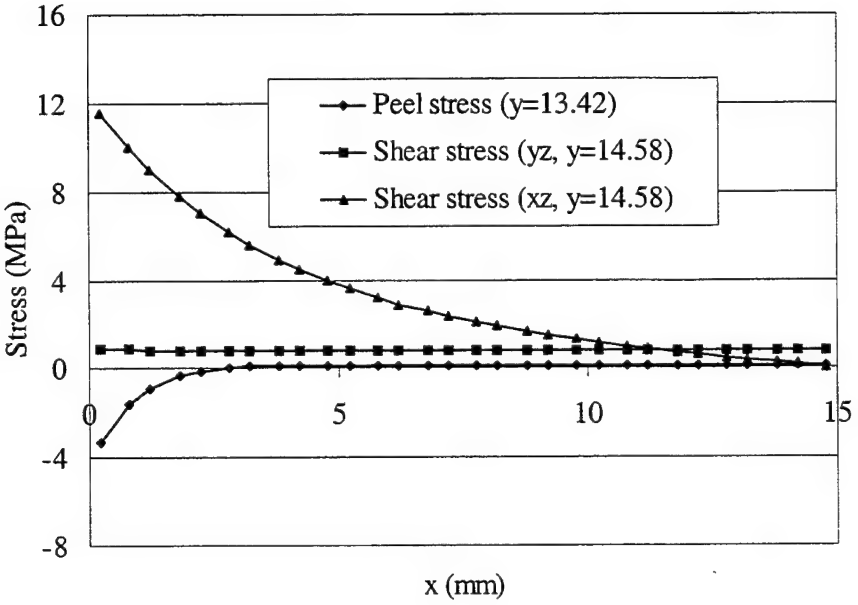

Figure 6-18 Stress distribution along x-axis with peak stress for the metallic cylindrical shell bonded two internal composite patches subjected to external pressure

In the columns of H_1=H_2=5 mm in Table 6-1 listed are the values and locations of peak stresses in the adhesive layer for various patching and loading combinations. It can be found from the columns in the table that for the same loading condition, a composite patch either internal or external yields a lower peak peel stress than a metallic patch. It is also evident that application of the combinations, namely, internal patch under external pressure and external patch under internal pressure, is more favorable than the other two.

6.4 Effect of shell and patch thickness

To study the effect of shell and patch thickness, another four cases of thickness combinations are investigated. These four cases are: H_1=5.0mm and H_2=2.5 mm, H_1=5.0 mm and H_2=1.25 mm, and H_1=H_2=2.5 mm as well as H_1=5.0mm and H_2=2.5 mm. Table 6.1 summarizes the values and locations of peak stresses for different combinations of patches and loading conditions. A comparison of the peak peel stresses indicates that, for all thickness combinations considered, internal patches under an external pressure and external patches under an internal pressure are more favorable than the other two. The peak peel stress or its absolute value tends to increase as the patch thickness is reduced from 5 mm to 2.5 mm and 1.25 mm for the following patching and loading combinations: (a) external patches and internal pressure; and (b) internal patches and external pressure. For the other two patching and loading combinations, i.e., internal patches plus external pressure, and external patches and internal pressure, the peak peel stress attains the lowest when H1=5.0mm and H2=2.5 mm comparing to the other two thickness combinations, H_1=H_2=5.0 mm and H_1=5.0 mm, H_2=1.25 mm. The lowest values are larger than that for the case of external patches under internal pressure.

For the patching and loading combinations: (a) external patches and internal pressure, (b) external patches and external pressure, and (c) internal patches and external pressure, the positive peak peel stress for the case of H_1=5 mm is much lower than that of H_2=2.5 mm when H_2 is kept as a constant of 2.5 mm. For example, for case (b), the peak stress is 15.7 MPa when H_1=5 mm and it becomes 103.2 MPa when H_1=2.5 mm.

The results listed in Table 6.1 clearly indicate that the patch thickness must be optimally design to match the parent shell structure in order to minimize the positive peel stress under a given loading condition.

Table 6-1 The value and location of peak stress for different patch and load

Patch Location	Load	$H_1 = 5.0mm,\ H_2 = 5.0mm$			$H_1 = 5.0mm,\ H_2 = 2.5mm$			$H_1 = 2.5mm,\ H_2 = 2.5mm$			$H_1 = 5.0mm,\ H_2 = 1.25mm$		
		Peel stress (MPa)	Shear stress (yz, MPa)	Shear stress (xz, MPa)	Peel stress (MPa)	Shear stress (yz, MPa)	Shear stress (xz, MPa)	Peel stress (MPa)	Shear stress (yz, MPa)	Shear stress (xz, MPa)	Peel stress (MPa)	Shear stress (yz, MPa)	Shear stress (xz, MPa)
External	Internal pressure	5.0 (A)	3.1 (B)	10.1 (B)	6.3 (B)	2.6 (B)	9.2 (B)	10.4 (D)	2.7 (B)	9.8 (B)	12.9 (D)	1.5 (C)	4.6 (B)
External	External pressure	28.6 (B)	-6.1 (B)	8.7 (B)	15.7 (B)	-5.9 (B)	7.0 (B)	103.2 (B)	-11.0 (B)	30.5 (B)	92.9 (B)	-6.0 (B)	20.6 (E)
Internal	Internal pressure	40.1 (B)	-8.4 (C)	-40.3 (B)	26.4 (D)	-5.2 (C)	-26.8 (B)	90.4 (B)	-22.5 (C)	-94.6 (B)	95.3 (B)	-16.4 (C)	-67.3 (B)
Internal	External pressure	-5.5 (B)	2.2 (B)	10.3 (B)	-6.2 (B)	1.8 (B)	9.4 (B)	-5.0 (D)	2.9 (B)	14.2 (B)	-10.0 (D)	2.1 (C)	9.5 (B)
External composite	Internal pressure	2.8 (B)	1.3 (B)	11.3 (B)	5.8 (D)	0.9 (C)	10.1 (B)	8.1 (D)	1.0 (B)	11.2 (B)	10.2 (D)	0.6 (C)	5.0 (B)
External composite	External pressure	25.2 (B)	-2.9 (B)	6.4 (B)	13.9 (B)	-2.3 (B)	6.0 (B)	82.4 (B)	-4.3 (B)	24.6 (B)	65.3 (B)	-2.0 (D)	14.1 (B)
Internal composite	Internal pressure	30.5 (B)	-3.8 (C)	-30.7 (B)	25.5 (B)	-2.3 (C)	-27.8 (B)	75.1 (B)	12.9 (C)	-96.9 (B)	82.1 (B)	-6.5 (C)	-66.7 (B)
Internal composite	External pressure	-3.3 (0.21, 13.42)	0.9 (B)	11.6 (B)	-6.2 (D)	0.6 (B)	10.3 (B)	-2.7 (B)	1.7 (B)	15.7 (B)	-8.3 (B)	1.0 (C)	10.2 (B)

Note: H_1 is the thickness of the cylindrical shell, H_2 is the thickness of the patch. All the stresses are evaluated at the Gaussian quadrature point.

Location Note: A(0.21, 11.42), B((0.21, 14.58), C(15.0,14.58), D(0.21, 13.42), E(2.79, 14.58)

6.5 Effect of patch length

To understand the effect of patch size on stresses in adhesive layer, numerical results are obtained for the shell with two external patches of eight extra lengths subjected to an external pressure. It is worth pointing out that all patches are square in shape. Figure 6-19 plots the peak or high stresses at location of x=0.21 and y=14.58 versus the patch length. Similarly, the peel stress is much larger than other two shear stresses. The peel stress initially increases with the length of the patch ranging from 30 to 60 mm, and then decreases with a further increase of the patch length ranging from 60 to 180 mm. It is evident that there may exist an optimum patch length for this particular problem that yields a minimum positive peel stress.

It should be noted that at the selected location, x=0.21 and y=14.58, the positive peel stress peaks when the patch length is less than 150 mm, and the location of the positive peel stress moves when patch length is very long. To illustrate this variation, Figure 6-20 depicts the full 3-D views for the peel stress for a patch length of 60, 120 and 180 mm respectively. As shown in Figure 6-20(c), the positive peel stress for a patch length of 180 mm is smaller than the other two shown in Figure 6-20(a) and (b). The patch length also affects the distribution patterns of the two shear stresses, which are also shown in Figure 6-20.

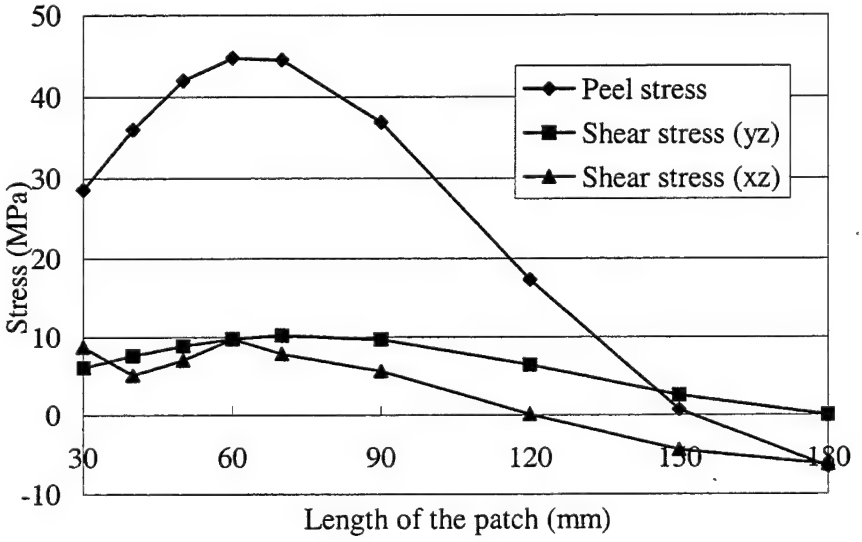

Figure 6-19 Stress (at x=0.21, y=14.58) for different length of the external patch subjected to external pressure load with $H_1 = 5.0mm$, $H_2 = 5.0mm$

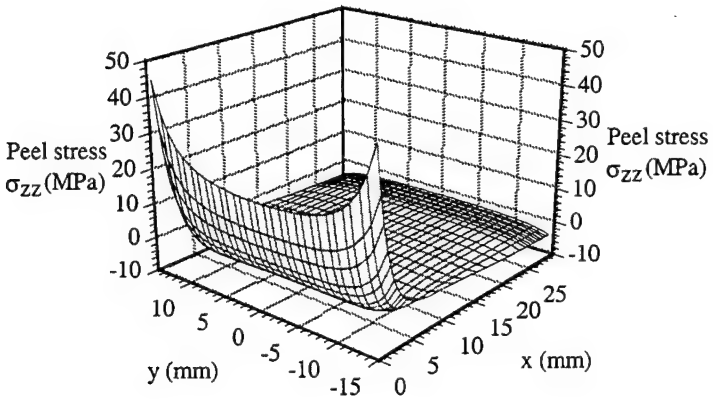

(a) Peel stress distribution (c=60mm)

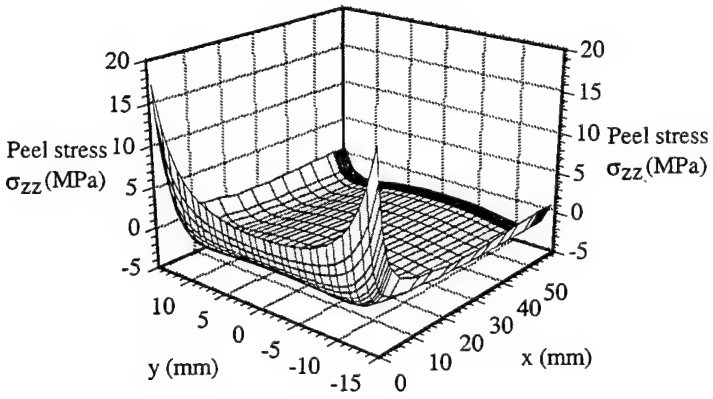

(b) Peel stress distribution (c=120mm)

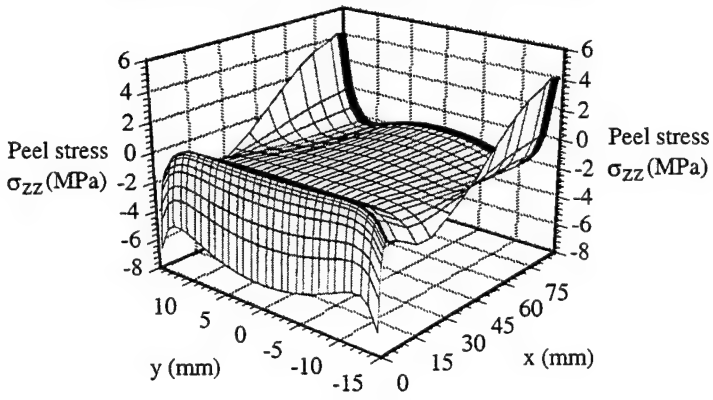

(c) Peel stress distribution (c=180mm)

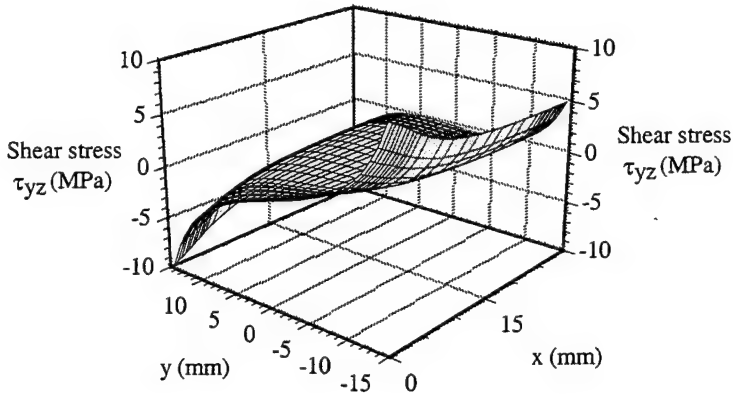

(d) Shear stress distribution (c=60mm)

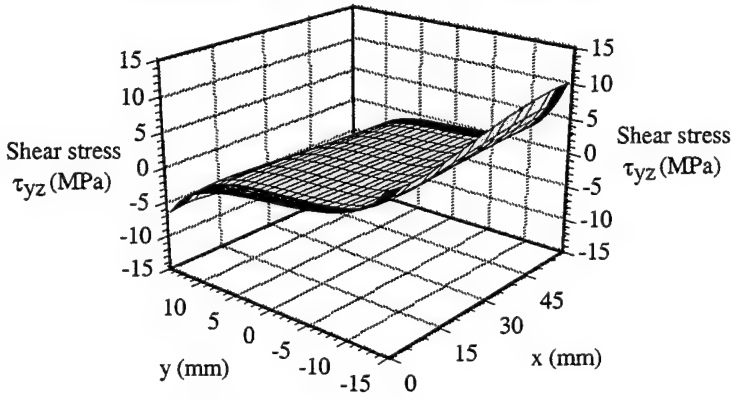

(e) Shear stress distribution (c=120mm)

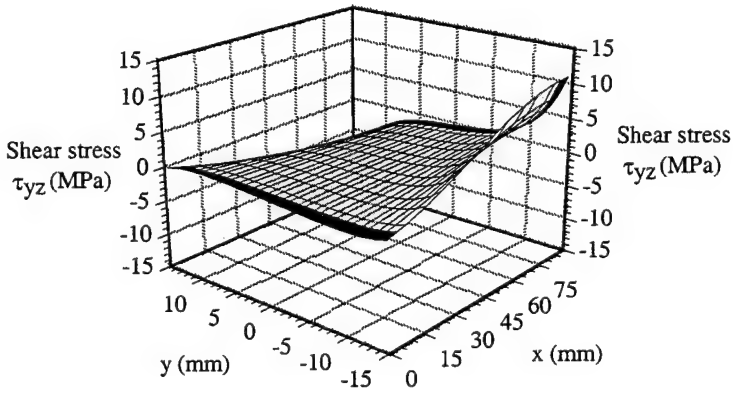

(f) Shear stress distribution (c=180mm)

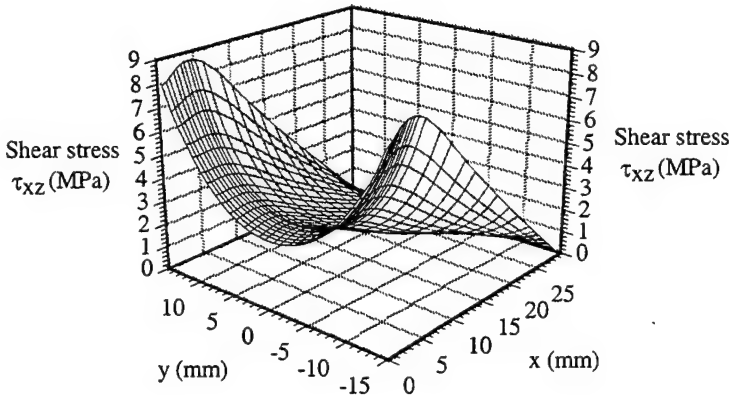

(g) Shear stress distribution (c=60mm)

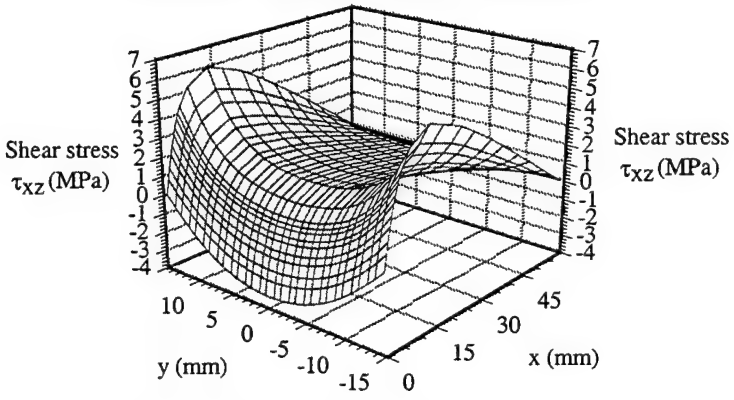

(h) Shear stress distribution (c=120mm)

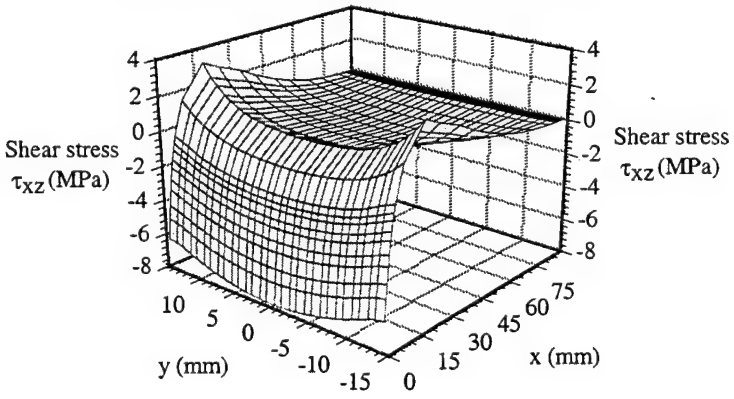

(i) Shear stress distribution (c=180mm)

Figure 6-20 Stress distribution for a cylindrical shell bonded two external patches with different length subjected external pressure load

7. NONLINEAR FINITE ELEMENT ANALYSIS

This section presents two formulations of nonlinear finite element analysis for bonded repair to curved thin-walled structures. One is for nonlinear finite element formulation when the thin-walled structures and patches undergo a large deformation, an the other one is when only the nonlinear adhesive behavior is taken into account in the nonlinear analysis. Numerical examples are given to illustrate the effect of nonlinearity on stresses in adhesive layer.

7.1. Formulation of large deformations

The large deformation formulation for the 4-node shell element, which is used in the 8-node adhesive element, is developed to investigate the effect of large deflection on stresses in adhesive layer. The Von Karman's nonlinear plate theory is used to take into account the moderately large deformations of the shell structure. Using this theory and following the finite element analysis procedure, the tangential element stiffness matrix can be written as:

$$[K_t] = [K_0] + [K_l] + [K_\sigma] \tag{40}$$

where $[K_0]$ is the linear stiffness matrix, $[K_l]$ is the geometric stiffness matrix due to large deformation, and $[K_\sigma]$ is the initial stress matrix. They are given by

$$[K_0] = \int_{-1}^{1}\int_{-1}^{1} [B_0]^T [D][B_0] |J| d\zeta d\eta \tag{41a}$$

$$[K_l] = \int_{-1}^{1}\int_{-1}^{1} \left([B_0]^T [D][B_l] + [B_l]^T [D][B_0] + [B_l]^T [D][B_l]\right) |J| d\zeta d\eta \tag{41b}$$

$$[K_\sigma] = \int_{-1}^{1}\int_{-1}^{1} [G]^T \begin{bmatrix} N_{xx} & N_{xy} \\ N_{xy} & N_{yy} \end{bmatrix} [G] |J| d\zeta d\eta \tag{41c}$$

in which $[B_0]$, $[B_l]$ and $[G]$ are the linear, nonlinear and geometric matrix respectively. N_{xx}, N_{yy} and N_{xy} are the membrane stress resultants. $|J|$ is the determinant of the Jacobian matrix, and $[D]$ is the material property matrix of the shell element as given in Section 3.

According to the relationship of strain-displacement in the shell element, matrix $[B_0]$, $[B_l]$ and $[G]$ can be defined as follows:

(a) Matrix $[B_0]$:

$$[B_0]=[B_{01} \quad B_{02} \quad B_{03} \quad B_{04}] \tag{42}$$

which is given in Section 4 in details.

(b) Matrix $[G]$:

$$[G]=[G_1 \quad G_2 \quad G_3 \quad G_4] \tag{43a}$$

where

$$[G_i]=\begin{bmatrix} 0 & 0 & N^0_{i,x} & 0 & 0 & 0 \\ 0 & 0 & N^0_{i,y} & 0 & 0 & 0 \end{bmatrix} \tag{43b}$$

(c) Matrix $[B_l]$:

$$[B_l]=[S][G] \tag{44}$$

$$[S]=\begin{bmatrix} w_{,x} & 0 & w_{,y} & 0 & 0 & 0 & 0 & 0 \\ 0 & w_{,y} & w_{,x} & 0 & 0 & 0 & 0 & 0 \end{bmatrix} \tag{45}$$

The tangential element stiffness matrix is first calculated in the local co-ordinate systems using the 2×2 Gaussian quadrature and then transformed into the global coordinate systems to assemble the total stiffness matrix. The well-known Newton-Raphson iteration scheme is employed to solve the nonlinear equilibrium equations in conjunction with a selected displacement convergence criterion.

7.2. Formulation including nonlinear adhesive behavior

It is assumed that the thin-walled structures and the patches exhibit linear elastic behavior while the adhesive layer is nonlinear hyperelastic. In this case, the stress-strain relation of the adhesive is nonlinear but the material behavior is elastic with all deformations and displacements recover when unloaded. It is also assumed that the peel and shear stress-strain curves can be used separately to replace the moduli E_A and G_A in Section 3. Figure 7.1 depicts a typical nonlinear stress-strain relations for FM-300 film adhesive [6].

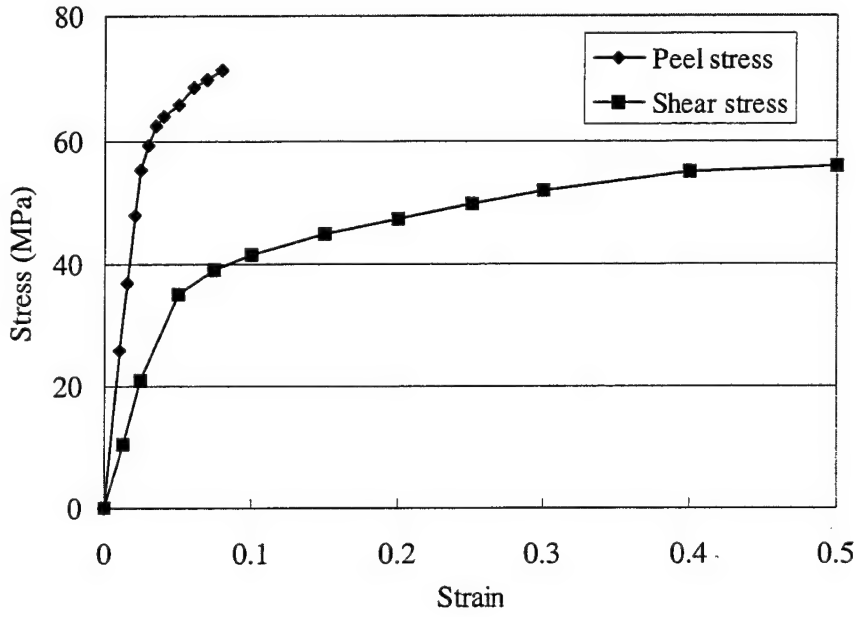

Figure 7-1. Typical peel and shear strain-stress curves for FM-300 film adhesive

An incremental iteration scheme is implemented in this section to take the individual peel and shear stress-strain curves into account in formulating the element stiffness matrix. For a general finite element analysis, the equilibrium equation of the structure can be written as:

$$Ku = P \tag{46}$$

where K is the total stiffness matrix, u is the displacement vector, P is the applied load vector.

To implement incremental iteration procedure, the applied loads are divided into several incremental steps. In each incremental step, the modified Newton-Raphson iteration method

is employed to calculate the incremental displacements at the current load level. The iterative procedure is detailed as follows.

1) Input data: defining geometry, loading, boundary conditions, material properties, etc.
2) Increment of the applied loads: $\Delta p = p/n$, where p is the total applied loads, n is the total number of incremental steps, Δp is the incremental loads. The current total loads are $P^i = \Delta P \times i$, where i is the number of the current increment step.
3) Residual forces ψ_{r-1}: the applied loads for the r^{th} iteration are the residual forces. $\psi_{r-1} = K(u_{r-1})u_{r-1} - P^i$, where $K(u)$ is the total stiffness matrix at the current displacements and u is the current total displacements. $K(u_{r-1})$ is formed based on the nonlinear elastic behavior. For r=1, $\psi_{r-1} = \Delta P$.
4) The tangent stiffness matrix: for each element, the elastic modulus is determined by it's stress level to form the tangent stiffness matrix K_r^i. For i=1, the tangent stiffness matrix is obtained assuming linear elastic behavior.
5) Compute the incremental displacement Δu_r: $\Delta u_r = [K_r^i]^{-1}\psi_{r-1}$.
6) Accumulate the total displacements for each element as $u_r = u_{r-1} + \Delta u_r$. Check to see if the solution has converged. If no, return to step c.
7) Check to see if the total loads are achieved. If no, return to step 2.
8) Output the results. The program is ended.

7.3. Numerical results and discussions

7.3.1. Effect of large deflection of the shell and patch structure

Geometrical nonlinear analysis of a metallic cylindrical shell bonded a composite patch subjected to various loads

Two geometrical configurations of bonded repairs are considered in this section. These Two types of bonded repairs are schematically depicted in Figure 7-2. An internally or externally reinforced composite patch is bonded to the shell. A though-thickness crack along the width of the shell is introduced in the middle span of the shell along the circumferential direction as shown in Figures 7-2.

In this section, the circular cylindrical shell is assumed to be metallic and has a Young's modulus of 70 GPa and a Poisson's ratio of 0.3. The adhesive has a Young's modulus of 2.4 GPa and a Poisson's ratio of 0.33. The composite patch is laminated using unidirectional carbon/epoxy tapes with all fibers aligned in the circumferential direction X. The nominal material properties of each ply are: E_1=131 GPa, E_2=E_3=11.2 GPa, G_{12}=G_{13}=6.55 GPa, G_{23}=4.375 GPa, μ_{12}=μ_{13}=μ_{23}=0.28. The geometric parameters are: L=150mm, arc length c=30mm, width of curved plate w=10mm, thickness of shell and patch H=5mm and adhesive thickness t=0.15mm.

Several types of loading and boundary conditions are considered for the above two geometrical configurations. There are two types of boundary conditions. In the first type of boundary condition, the vertical displacements at both ends of the circular cylindrical shells are assumed to be zero, this is referred to as BC1. In the second one, both vertical and horizontal displacements at both ends of the circular cylindrical shells are assumed to be zero, which is referred to as BC2. Three loading cases were considered. In load case 1, a uniformly distributed load of 60 N/mm along the width of the circular cylindrical shell is applied at both ends of the bonded repair in the outwards horizontal direction. In load case 2, a uniformly distributed moment of 60 N along the width of the shell is applied at both ends of the shell. In load case 3, an internal pressure of 1 MPa is applied to the bonded repair. The three load cases are schematically depicted in all figure plots peak stresses versus the curvature.

Three illustrative examples are considered by combining with various geometric configurations, loading and boundary conditions. The first two example are combination of load case 1 and 2 with boundary condition case 1 (BC1), while the third example is a combination of load case 3 and boundary condition BC2.

Due to symmetry in geometry, material and all applied loads, only half of structure of the bonded repair shown in Figure 7-2 is modeled using the newly developed finite element analysis program. Along the half arc length of the bonded area 60 elements of equal length were used, and two elements were used in the width direction. Both linear and geometrical nonlinear finite element analyses are performed for all cases. In all calculations, it is assumed that both shell adherends have the same radius of curvature, denoted by R, as shown in Figure

7-2. When R is infinite both adherends become flat, which represent the typical single-side bonded repair with flat adherends. When R has a finite value the curvature of the shell is given by $1/R$. In the presentation of the effect of curvature on stresses for the three examples, peak stresses in adhesive layer are plotted versus the value of $1/R$.

(a) Example 1: A curved shell with a bonded patch subjected to tensile load

In this example, a circular cylindrical shell with an internally or externally bonded patch is assumed to be subjected to a tensile load in the outward horizontal direction (see the embedded drawing in Figures 7-3 and 7-4 at the both ends of the shell. Figures 7.3 and 7.4 plot the peak peel and shear stresses in the adhesive layer for the externally and internally patched circular cylindrical shell with a crack. All solid lines represent the linear finite element analysis results, while all dashed lines are the nonlinear finite element analysis results. The "left" denotes the left end of the adhesive layer while the "middle" means the right end to the crack in the middle when half of the structure is modeled only. From this example, it is evident that the peak peel and shear stresses predicted by taking into account the large deflections are significantly lower than those obtained using linear finite element analysis. Another important finding is that the value of curvature 1/R has a profound effect on the peak stresses, namely, the larger the value of curvature 1/R, the greater the absolute value of the peak stresses.

Comparison of Figures 7-3 and 7-4 reveals that: (a) the peak peel stress predicted in the case of externally bonded patch is smaller than that of internally bonded patch; (b) the absolute value of the peak shear stress for the case of externally bonded patch is larger than that of the internally bonded patch. As peel stress is generally regarded as more detrimental to the bonding strength than shear stress, it is thus believed that an externally bonded composite patch may be more adequate than the internal one for the case considered.

(b) Example: 2 A curved shell with a bonded patch subjected to pure bending moment

In this example, we assume that a circular cylindrical with an internally or externally bonded patch is subjected to a uniformly distributed bending moment (see the embedded drawing in Figures 7-5 and 7-6) at the both ends of the shell. Figures 7-5 and 7-6 plot the peak peel and shear stresses in the adhesive layer for the externally and internally patched circular

cylindrical shell with a crack. It is interesting to find that the value of curvature does not seem to influence the peak peel and shear stresses for the loading and boundary conditions considered. Further numerical results show that this is true for both cases of with and without crack in the middle span of the shell. The peak peel stress for the case with an externally bonded patch is lower than that with an internally bonded patch for the configuration with a crack under the considered loading and boundary conditions. It is worth pointing out that there exists a negligible difference between the linear and nonlinear results.

(c) Example 3: A curved shell with a bonded patch subjected to internal pressure load

This example considers the case when a shell with a bonded patch is subjected to internal pressure load and fixed at both ends. Figures 7-7 and 7-8 plot the peak peel and shear stresses in the adhesive layer for the externally and internally patched circular cylindrical shell without and with a crack under an applied internal pressure. The line types and marks used in this example are the same as those used in example 1. It is evident the effect of curvature on the absolute values of the peak stresses is significant. The absolute values of peak stresses tend to significantly decrease and the effect of geometrical nonlinearity becomes slightly less significant when the value of curvature 1/R is increased from 1/750 to 1/150.

Comparison of the peak peel stresses in Figure 7-7 and 7-8 unveils that maximum positive peel stress occurs at the middle end near the crack for both cases with an internally and externally bonded patch. The peak peel stress for the case with an internally bonded patch is actually larger than that for the case with an externally bonded patch. For example, when R=750, the linear analysis results show that the maximum peel stress near the crack for the case with an internally bonded patch is 25% larger than that for the case with an externally bonded patch. The results of this example indicate that an externally bonded patch is probably more adequate than an internally bonded patch under the considered loading and boundary conditions.

(d) Example 4: A curved shell with a bonded patch subjected to an external pressure

In this example, the cylindrical shell with a bonded patch is subjected to an external pressure and fixed at both ends. Figures 7-9 and 7-10 plot the peak peel and shear stresses in the

adhesive layer for the externally and internally patched circular cylindrical shell with a crack under an external pressure. Only the results of linear analysis are presented as snap-through buckling can occur when large deflection is included. Evidently, the effect of curvature on the absolute values of the peak stresses is significant. Similar to the previous case, the absolute values of peak stresses significantly decrease when the value of curvature 1/R is increased from 1/750 to 1/150. Comparison of the peak peel stresses reveals that maximum positive peel stress occurs at the left end for the case with an internal patch. Similarly to the previous example, The results of this example indicate that an externally bonded patch is probably more favorable than an internally bonded patch.

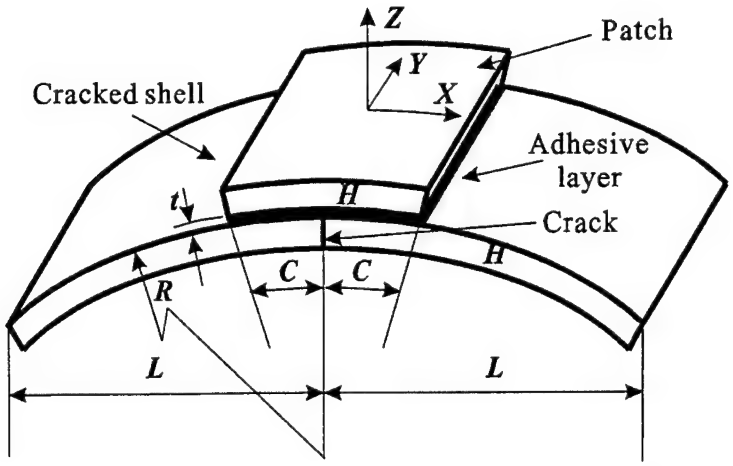

(a) A cracked cylindrical shell with an externally boned patch

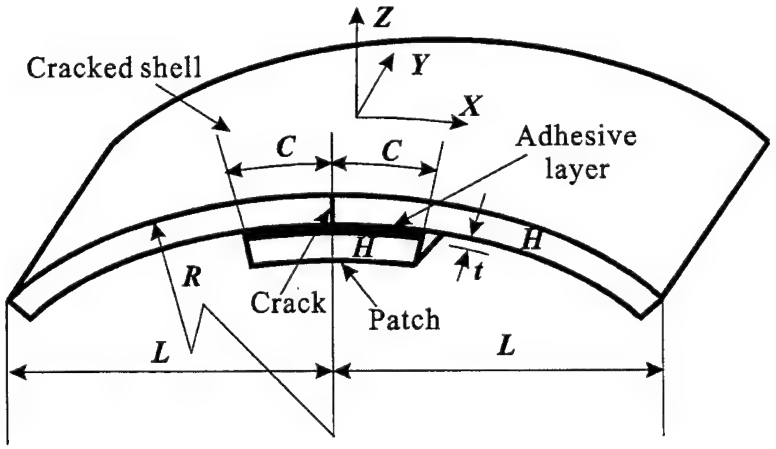

(b) A cracked cylindrical shell with an internally boned patch

Figure 7-2 Two types of bonded repair configurations.

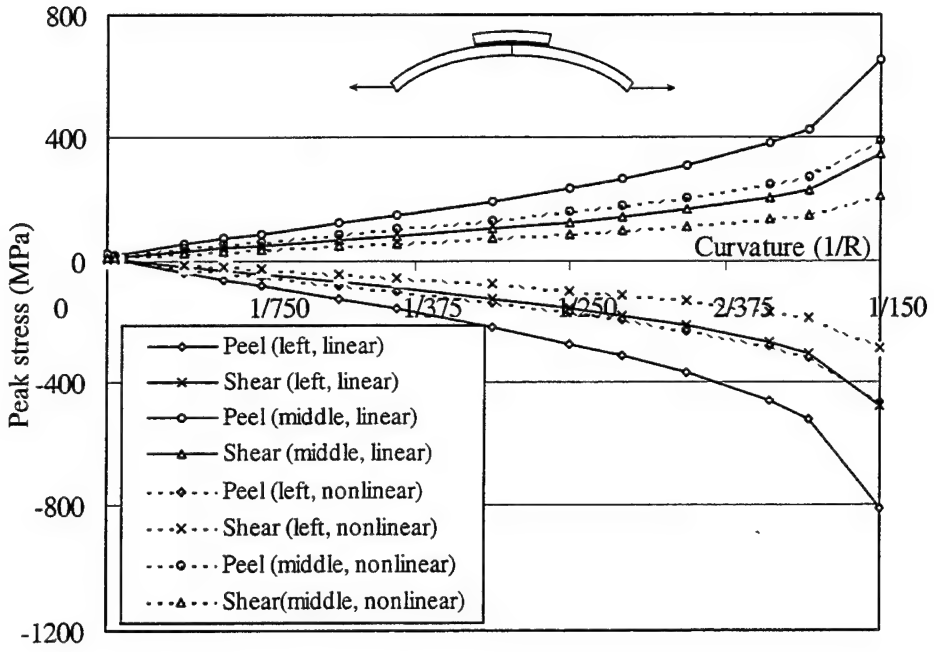

Figure 7-3 Peak peel and shear stresses in adhesive in the cracked cylindrical shell with an externally bonded patch versus curvature

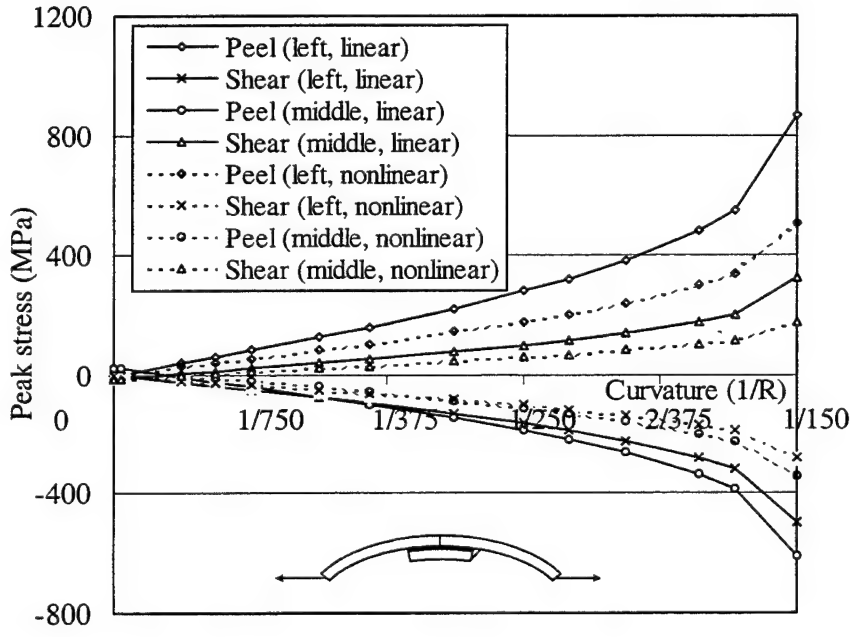

Figure 7-4 Peak peel and shear stresses in adhesive in the cracked cylindrical shell with an internally bonded patch versus curvature

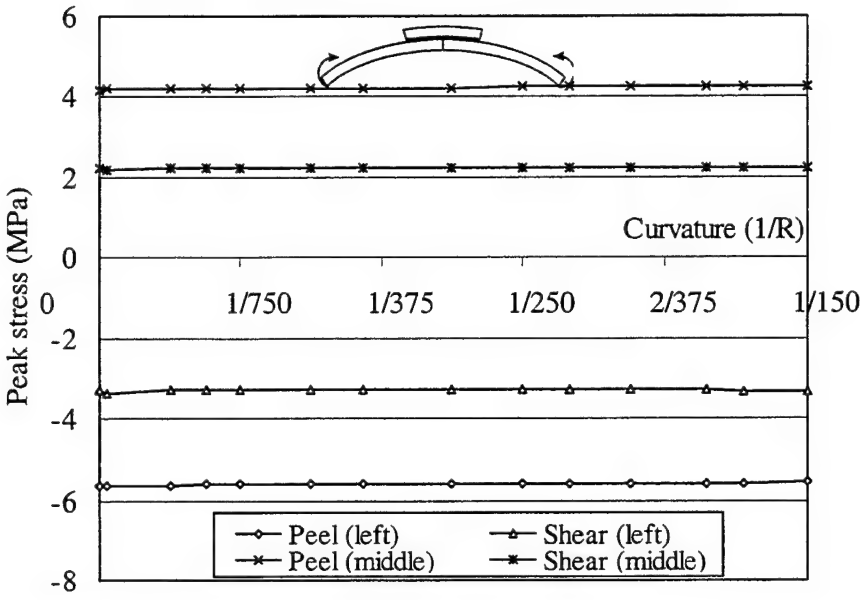

Figure 7-5 Peak peel and shear stresses in adhesive in the cracked cylindrical shell with an externally bonded patch versus curvature with an internally bonded patch versus curvature

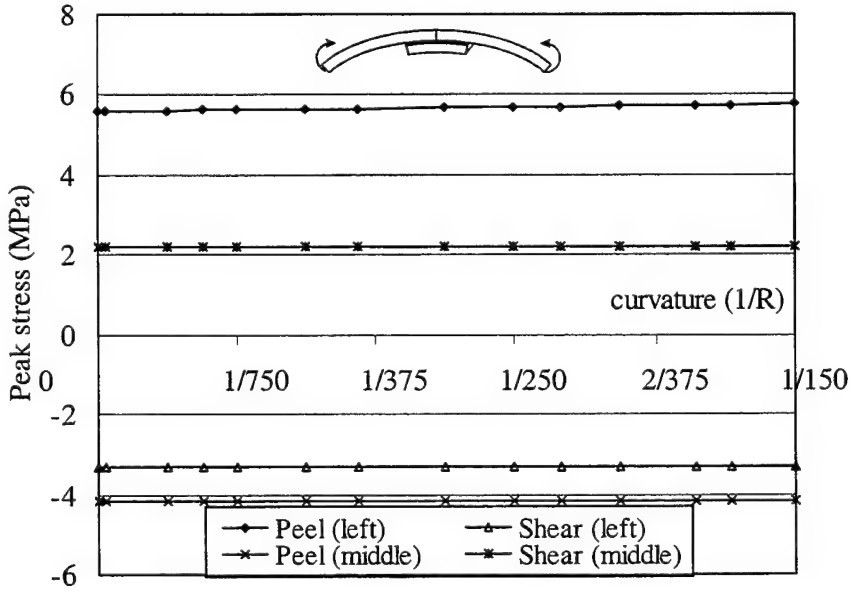

Figure 7-6 Peak peel and shear stresses in adhesive in the cracked cylindrical shell with an internally bonded patch versus curvature

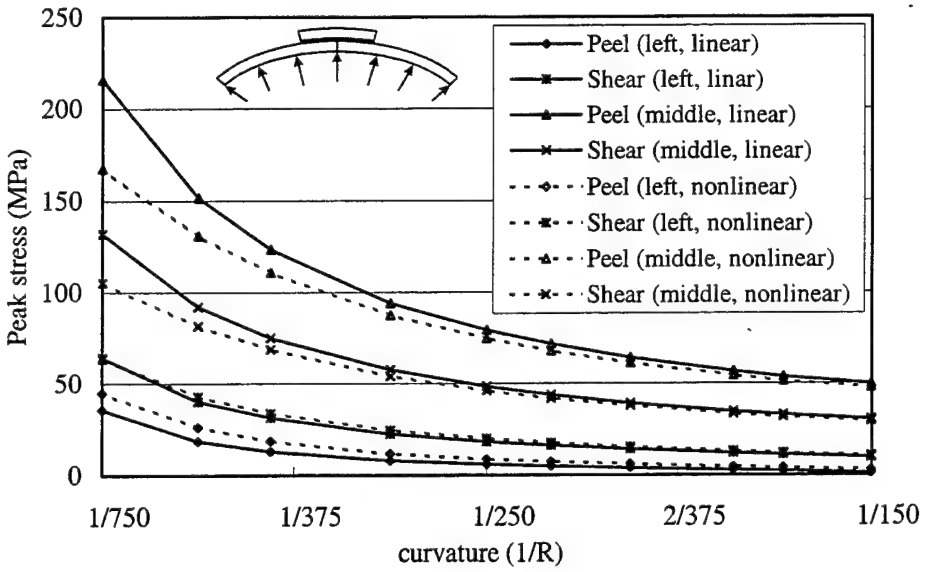

Figure 7-7 Peak peel and shear stresses in adhesive at the left end in the cracked cylindrical shell with an externally bonded patch subject to an internal pressure versus curvature

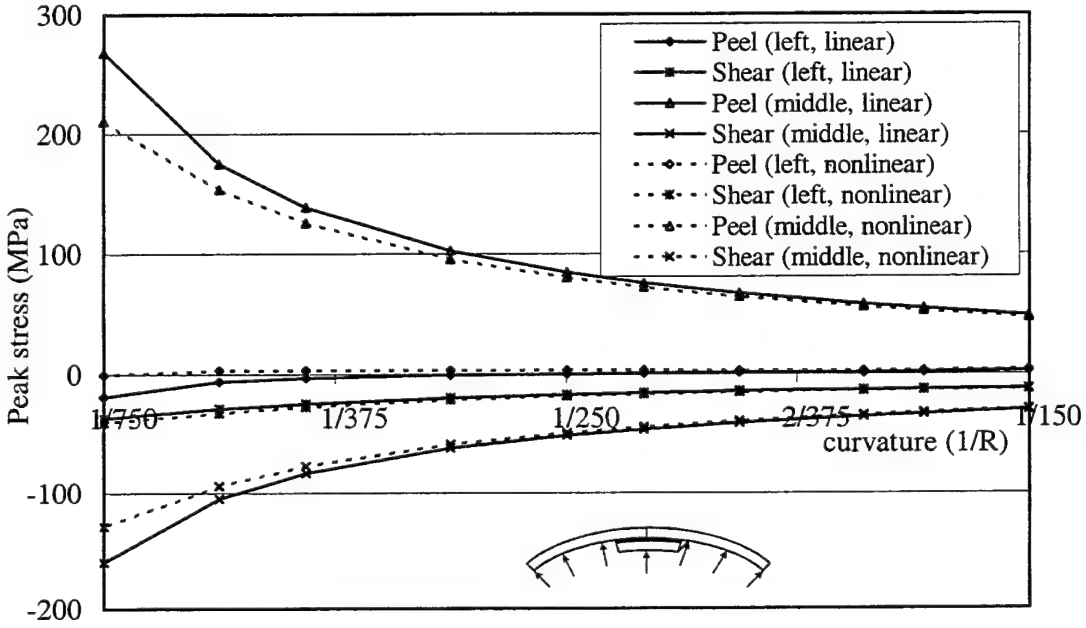

Figure 7-8 Peak peel and shear stresses in adhesive at the left end in the cracked cylindrical shell with an externally bonded patch versus curvature

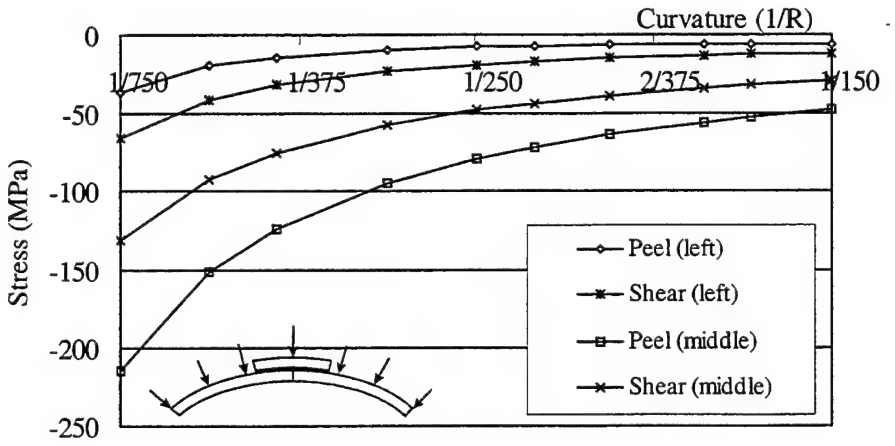

Figure 7-9 Peak peel and shear stresses in adhesive at the middle (cracked end) in the cracked cylindrical shell with an externally bonded patch under an external pressure versus curvature

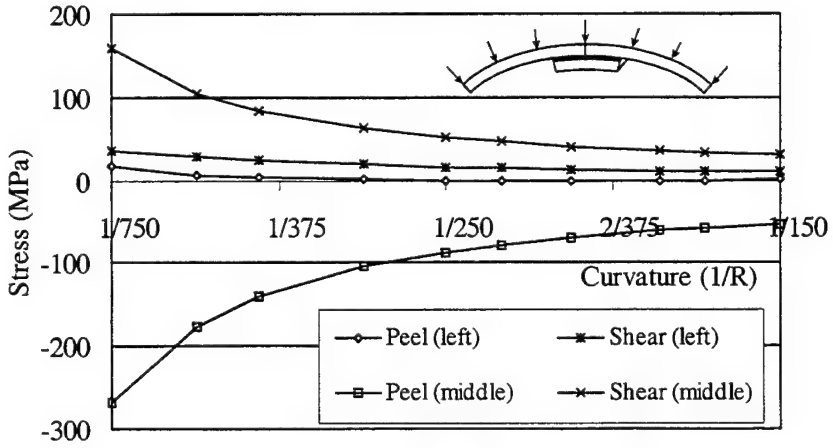

Figure 7-10 Peak peel and shear stresses in adhesive at the middle (cracked end) in the cracked cylindrical shell with an internal patch under an internal pressure versus curvature

7.3.2. Effect of adhesive nonlinear behavior

In this case, the typical adhesive stress-strain curves for the FM-300 film adhesive as shown in Figure 7-1 are used in all calculations.

(a) Example 5

In this example, a non-cracked circular cylindrical shell is bonded with an external patch. It has the same geometrical configuration as that shown in Figure 7-2(a) except that no crack exists in the middle of the shell, and the same boundary conditions. A uniformly distributed tensile load of 30 N/mm is applied along both ends of the shell at five equal load increments. The radius of curvature of the shell is taken as R=300 mm. Both the shell and patch are metallic be metallic with a Young's modulus of 70 GPa and a Poisson's ratio of 0.3. Figure 7-11 compares the distributions of both peel and shear stresses in adhesive layer along half of the bonded length in the circumferential direction obtained using linear and nonlinear adhesive properties. It is seen that for this example both peel and shear stresses at the left end are significantly affected by the nonlinear adhesive properties. Figure 12 plots the peak peel and shear stresses at the left end versus the applied load. This figure clearly shows that when nonlinear adhesive bahavior becomes effective when the applied load is above 10 N/mm.

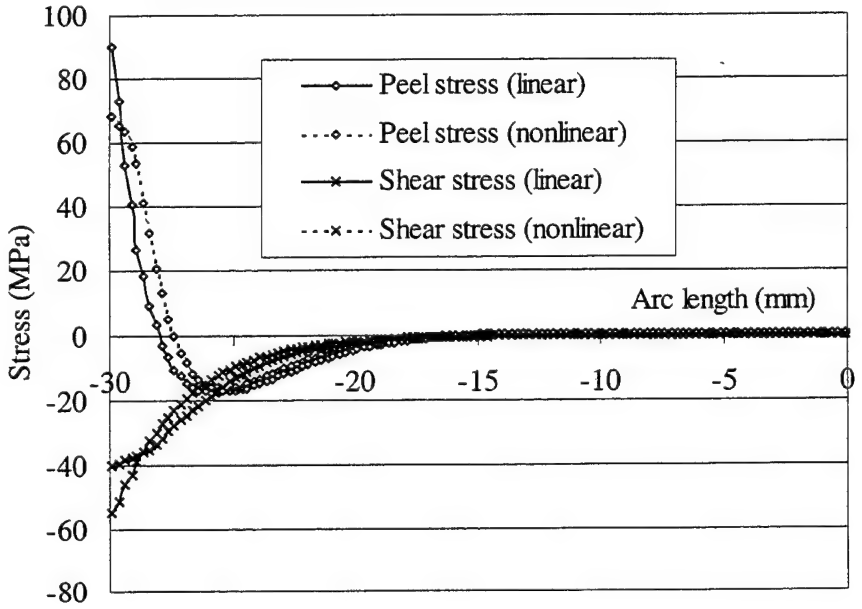

Figure 7-11 Stress distribution in bondline for a continuous plate/shell with an externally bonded patch loaded in tension at both ends (P=30.0N/mm)

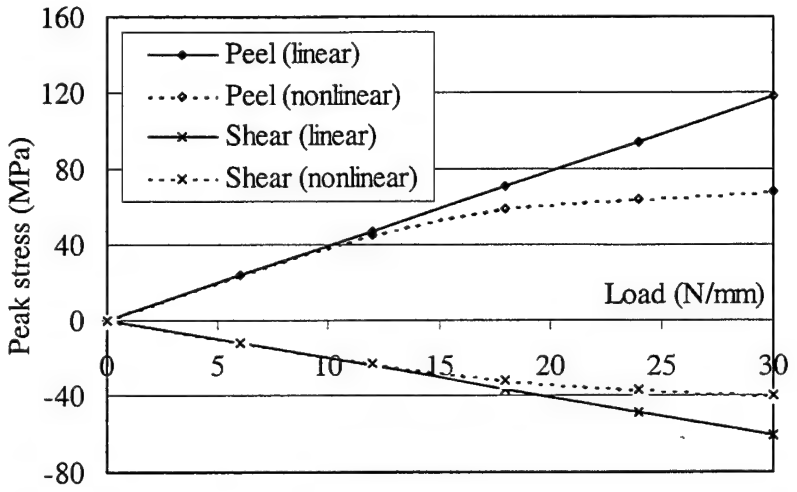

Figure 7-12 Peak stress at different load level for a continuous plate/shell with an externally bonded patch loaded in tension at both ends (P=30.0N/mm)

(b) Example 6

In this example, we consider the circular cylindrical shell with two symmetric bonded patches as defined in Section 6.2 and 6.3. Both ends of the shell are supported by rigid diaphragms, which allow displacement only in the axial direction of the shell. Due to symmetry, only one quarter of the structure is modeled using fine mesh near the periphery of the patch and coarse mesh in the remaining area. All geometrical and material properties are the same as those used in Section 6.2 and 6.3, except that the nonlinear peel and shear stress-strain curves are employed in this example. Two types of patch combinations are considered, namely, both patches are either externally or internally bonded. Two of materials are selected for the bonded patches, and they are metal and composite materials. The material properties are the same as those used in Section 6.2 and 6.3. Two load cases, i.e., internal pressure and external pressure, are considered. The applied pressure is 5 MPa, which is applied to the structure at equal five load increments, namely, p=1.0, 2.0, 3.0, 4.0 and 5.0MPa. All together eight problems are analyzed in this example, namely, 2 loading cases for 4 geometrical and material configurations.

Figures 7-13 to 7-15 depict the contours of the peel and two shear stresses over half of the bonded patch obtained by assuming linear and nonlinear adhesive properties. It is evident that nonlinear adhesive behavior can significantly influence the peak stresses, particularly the peak peel stresses in this example. However, material nonlinearity does not seem to greatly change the topologies of the stress distributions.

Figures 16 and 17 depict the distributions of the peel stress and two shear stresses along the longitudinal direction from y=-15 to y=15 at one patch edge x=0 and along the circumferential direction from x=0 to x=15 near the patch edge y=14.58. Both figures show that there exists a significant difference only in the peel stress between the linear and nonlinear analyses.

Table 7.1 summarizes the maximum peel and shear stresses for the eight problems solved using linear and nonlinear finite element analysis procedure incorporating nonlinear adhesive behavior. Similarly, consideration of nonlinear adhesive behavior tends to reduce peak stresses dramatically. For this example, the peak peel stress can be reduced up to 50%. An comparison of all peel stresses unveils that for considered metallic and composite patches, external patching is preferred when the shell is subjected to an internal pressure and internal patching is preferred when subjected to an external pressure.

Table 7-1 The values and loci of linear and nonlinear peak stresses in the adhesive*

Patch	Load	Linear stress			Nonlinear stress		
		Peel stress σ_{zz} (MPa)	Shear stress τ_{yz} (MPa)	Shear stress τ_{xz} (MPa)	Peel stress σ_{zz} (MPa)	Shear stress τ_{yz} (MPa)	Shear stress τ_{xz} (MPa)
External metallic	external	148.0 (A)	29.2 (A)	42.5 (A)	70.8 (A)	24.4 (A)	35.1 (A)
External metallic	internal	25.4 (B)	14.9 (A)	49.0 (A)	24.7 (B)	11.6 (A)	37.1 (A)
Internal metallic	external	-28.3** (D)	10.9 (A)	50.0 (A)	-27.0 (D)	8.6 (A)	36.3 (A)
Internal metallic	internal	207.4 (A)	-25.2 (A)	-147.4 (A)	71.5 (A)	-12.2 (A)	-51.3 (A)
External composite	external	130.2 (A)	-14.0 (A)	31.0 (A)	70.1 (A)	-12.1 (A)	27.5 (A)
External composite	internal	14.2 (C)	6.6 (A)	54.7 (A)	13.5 (C)	5.4 (A)	38.4 (A)
Internal composite	external	-16.8** (D)	4.4 (A)	55.9 (A)	-15.8 (D)	3.7 (A)	38.8 (A)
Internal composite	internal	156.7 (A)	-8.3 (A)	-148.2 (A)	71.5 (A)	-6.2 (A)	-51.3 (A)

*The upper case letters in the brackets indicate the values of the x and y coordinate at the following point: A(14.58, 14.58); B(0.21, 11.42); C(0.21, 12.58); D(0.21, 13.42)

** Negative peel stress indicates that there is no positive peel stress or the positive peel stress is negligible.

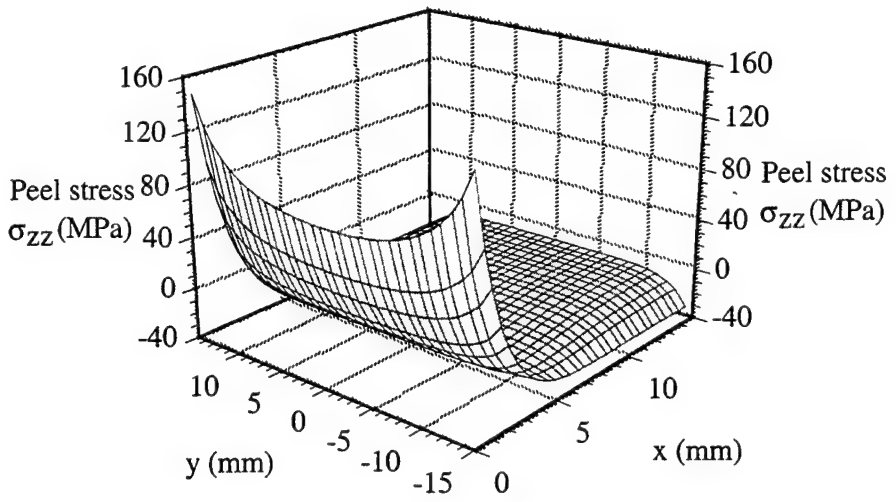

(a) Linear analysis

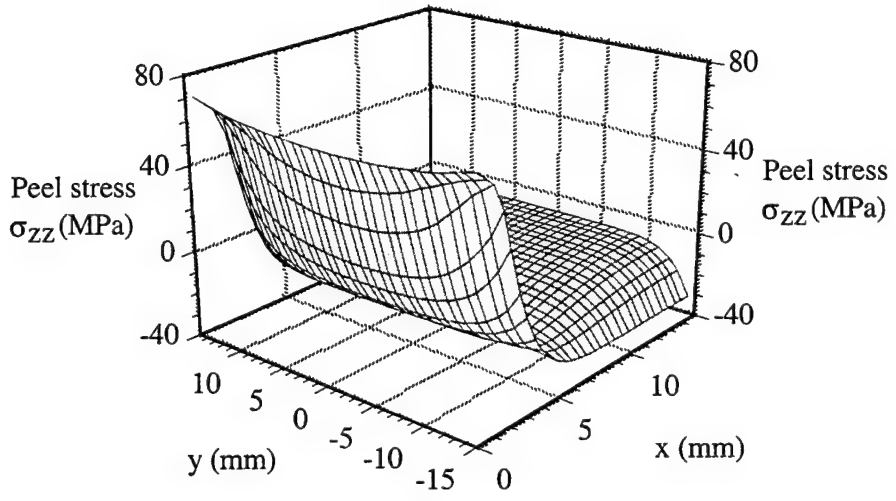

(b) Nonlinear analysis

Figure 7-13 Peel stress distributions for the shell with external patches under external pressure of 5.0MPa, (a) linear analysis, and (b) nonlinear analyses

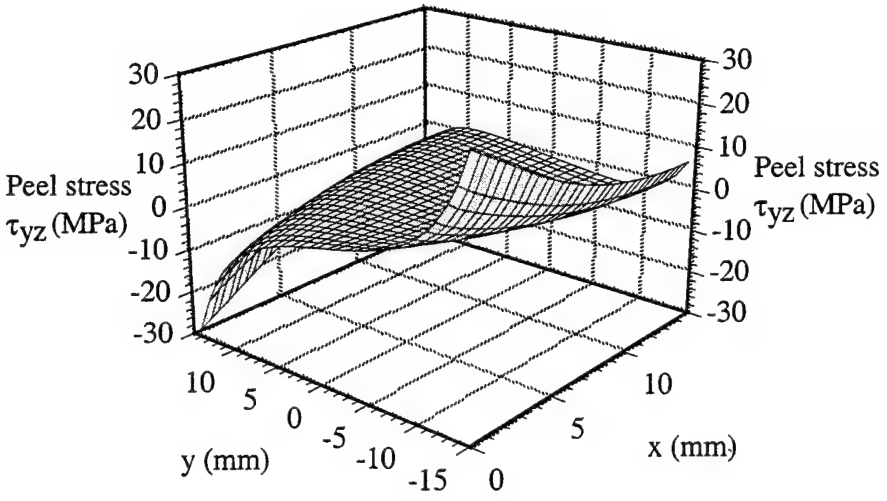

(a) linear analysis

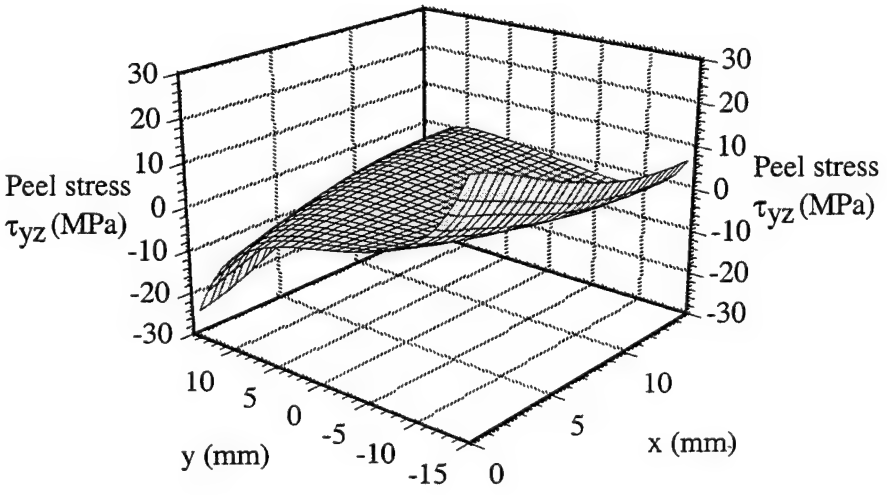

(b) Nonlinear analysis

Figure 7-14 Shear stress distribution for the shell with external patches under external pressure of 5.0MPa, (a) linear analysis, (b) nonlinear analysis

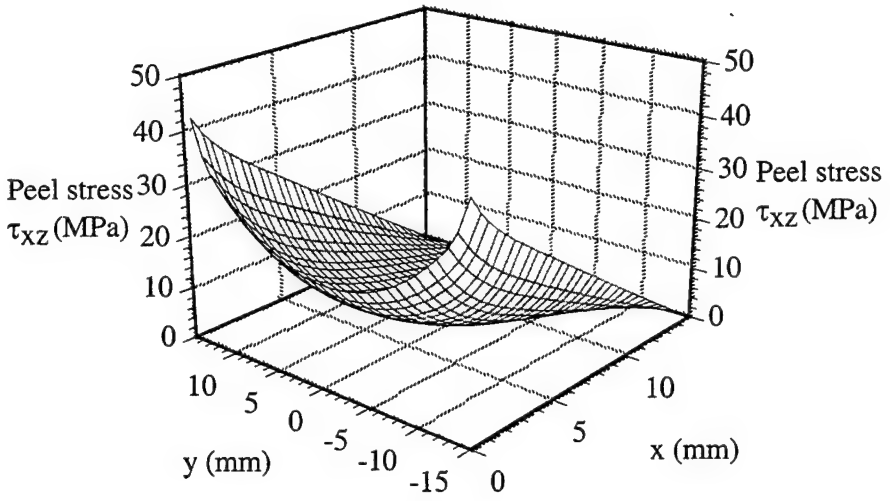

(a) linear

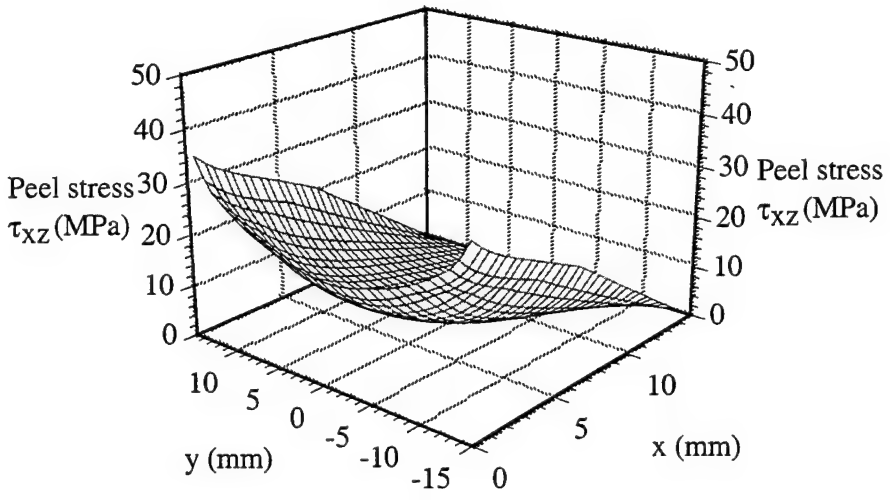

(b) Nonlinear

Figure 7-15 Shear stress distribution for the shell with external patches under external pressure of 5.0MPa, (a) linear analysis, (b) nonlinear analysis

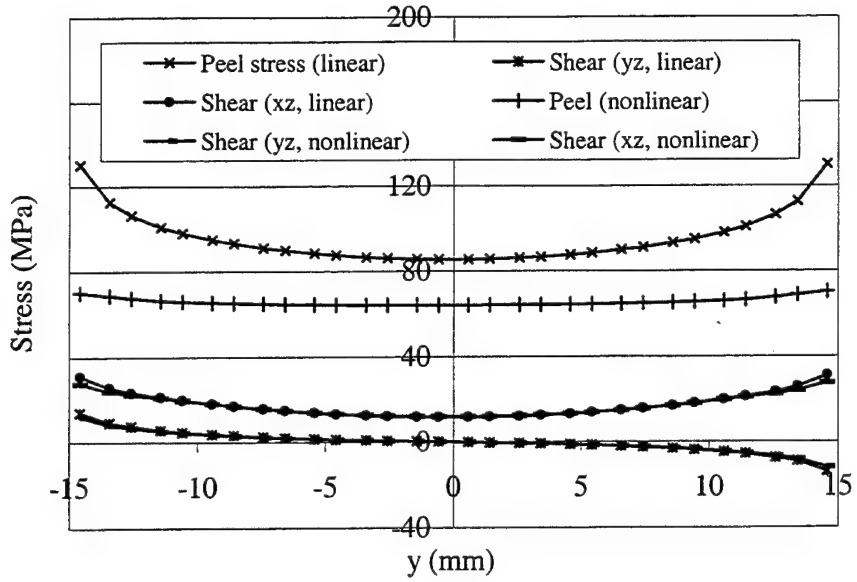

Figure 7-16 Stress distribution along y-axis at x=0 for the shell with two external patches under an external pressure of 5.0MPa)

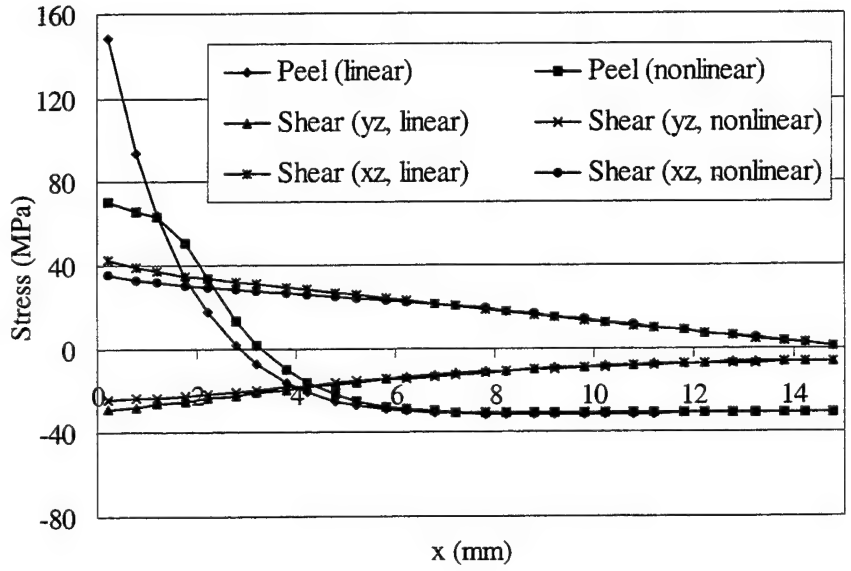

Figure 7-17 Stress distribution along x-axis at y=14.58 for the shell with two external patches under an external pressure of 5.0MPa)

8. THERMAL STRESS ANALYSIS

In this section, thermal stress analysis is performed for the thin-walled structures with bonded patches.

8.1. Fundamental formulation

The relationship between stress and strain of any ply in a composite shell can be expressed as:

$$\begin{Bmatrix}\sigma_x\\ \sigma_y\\ \tau_{xy}\\ \tau_{yz}\\ \tau_{zx}\end{Bmatrix}=\begin{bmatrix}\overline{Q}_{11} & \overline{Q}_{12} & \overline{Q}_{16} & 0 & 0\\ \overline{Q}_{21} & \overline{Q}_{22} & \overline{Q}_{26} & 0 & 0\\ \overline{Q}_{61} & \overline{Q}_{62} & \overline{Q}_{66} & 0 & 0\\ 0 & 0 & 0 & \overline{Q}_{44} & \overline{Q}_{45}\\ 0 & 0 & 0 & \overline{Q}_{54} & \overline{Q}_{55}\end{bmatrix}\begin{Bmatrix}\varepsilon_x-\alpha_x\Delta T\\ \varepsilon_y-\alpha_y\Delta T\\ \varepsilon_{xy}-\alpha_{xy}\Delta T\\ \gamma_{yz}\\ \gamma_{zx}\end{Bmatrix} \tag{47}$$

where $\overline{Q}_{ij}(i,\ j=1,\ 2,\ 4,\ 5,\ 6)$ are the off-axis stiffness coefficient, $\alpha_x, \alpha_y, \alpha_{xy}$ are the off-axis coefficient of thermal expansion and ΔT is the temperature change.

The relationship between the off-axis and on-axis coefficient of thermal expansion is:

$$\begin{aligned}\alpha_x &= \alpha_1\cos^2\theta+\alpha_2\sin^2\theta\\ \alpha_y &= \alpha_1\sin^2\theta+\alpha_2\cos^2\theta\\ \alpha_{xy} &= 2(\alpha_1-\alpha_2)\sin\theta\cos\theta\end{aligned} \tag{48}$$

where α_1 and α_2 are the longitude and cross on-axis coefficient of thermal expansion, respectively. θ is the ply angle.

Then the stress resultants in the cross-section of shell can be expressed as:

$$\begin{Bmatrix}N\\ M\\ Q\end{Bmatrix}=\begin{bmatrix}A & B & 0\\ B & D & 0\\ 0 & 0 & H\end{bmatrix}\begin{Bmatrix}\varepsilon\\ \kappa\\ \gamma\end{Bmatrix}-\begin{Bmatrix}N^T\\ M^T\\ 0\end{Bmatrix} \tag{49}$$

where N, M, Q are the membrane, moment and shear stress resultants, respectively. A, B, D, H are defined as equation (3) in Section 3.2. ε, κ and γ are membrane, bending and shear strain. N^T, M^T are membrane and moment resultants caused by temperature change, which are defined as follows,

$$\left(N_i^T, M_i^T\right) = \int_{-h/2}^{h/2} \overline{Q}_{ij}(1, z)\alpha_j \Delta T dz \qquad (i, j = 1, 2, 6) \tag{50}$$

where h is the thickness of shell.

The equilibrium equation can be written as:

$$[K]\{q\} = \{F\} + \{R\} \tag{51}$$

where $[K]$ is the stiffness matrix:

$$[K] = \int_A [B]^T \begin{bmatrix} A & B & 0 \\ B & D & 0 \\ 0 & 0 & H \end{bmatrix} [B] dA \tag{52}$$

$[B]$ is the geometric matrix, A is the area of the element. $\{q\}$ is the displacement vector. $\{F\}$ is the applied load vector. $\{R\}$ is the thermal load vector cased by temperature change, which is

$$\{R\} = \int_A [B]^T \begin{Bmatrix} N^T \\ M^T \\ 0 \end{Bmatrix} dA \tag{53}$$

8.2. Numerical results and discussion

Thermal stress analyses of the same bonded circular cylindrical shells as described in Section 6.2 and 6.3 are performed. The temperature change in the adhesive layer is not considered in the analysis. The following six cases are analyzed

1) Metallic shell with external metal patches.
2) Metallic shell with internal metal patches.
3) Metallic shell with external composite patches.
4) Metallic shell with internal composite patches.
5) Composite shell with external composite patches.
6) Composite shell with internal composite patches.

All material properties used are the same as those in Section 6.2 and 6.3. The coefficient of thermal expansion of the metallic material is assumed to be $\alpha = 0.23\times10^{-4}$. The coefficients of thermal expansion of the composite material are taken as $\alpha_1 = -6.3\times10^{-8}, \alpha_2 = 2.88\times10^{-5}$, in which subscript 1 indicates the fiber direction and subscript 2 the transverse direction. The applied thermal loading is temperature change from $220^\circ C$ down to $20^\circ C$.

Figures 8-1 to 8-6 plot the three stresses along (a) the y-axis at x=0 and (b) the x-axis at y=14.58 for the above six cases. As shown in Figures 8-1 and 8-2, the peak peel stress is positive for case 2 and negative for case 1, and thus external metallic patches are more preferred than the internal ones. For case 3 and 4, there seems to be no difference between the peak peel stresses, which are significantly high than those of the first two cases. This may indicate that there exists no difference between internal and external patching from the point of view of peel stress. For the last two cases, when both parent shell and patches are both composites, similar to the first two cases, external patching is more favorable than internal patching.

It is worth pointing out that composite patching to a metallic shell creates very high peel stress comparing to metallic patching to a metallic shell and composite patching to a composite shell.

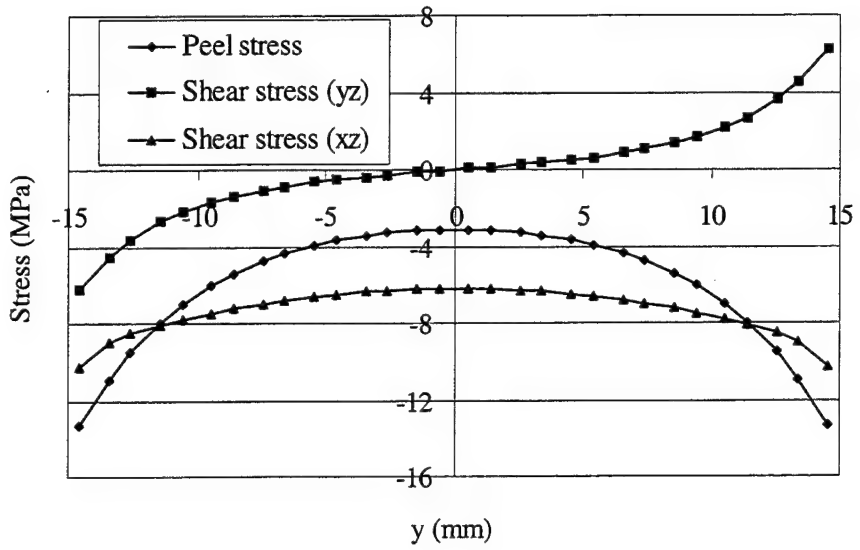

Figure 8-1(a) Thermal stress distribution along y-axis at x=0 for the metallic cylindrical shell with external metallic patches

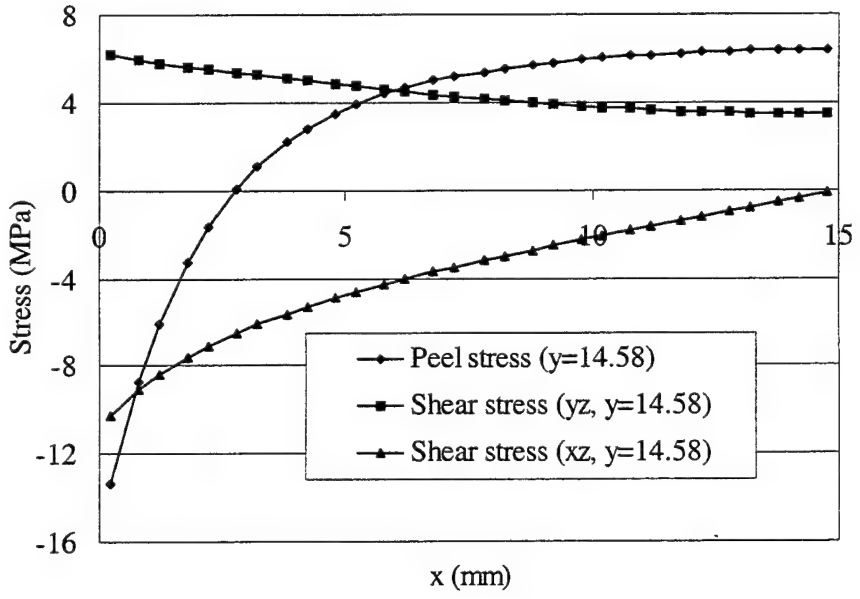

Figure 8-1(b) Thermal stress distribution along x-axis with peak stress for the metallic cylindrical shell with external metallic patches

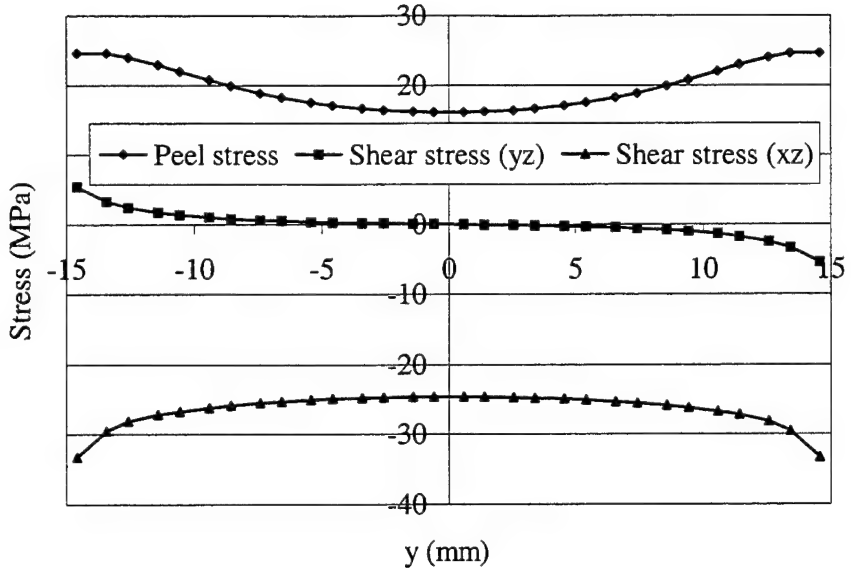

Figure 8-2(a) Thermal stress distribution along y-axis at x=0 for the metallic cylindrical shell with internal metallic patches

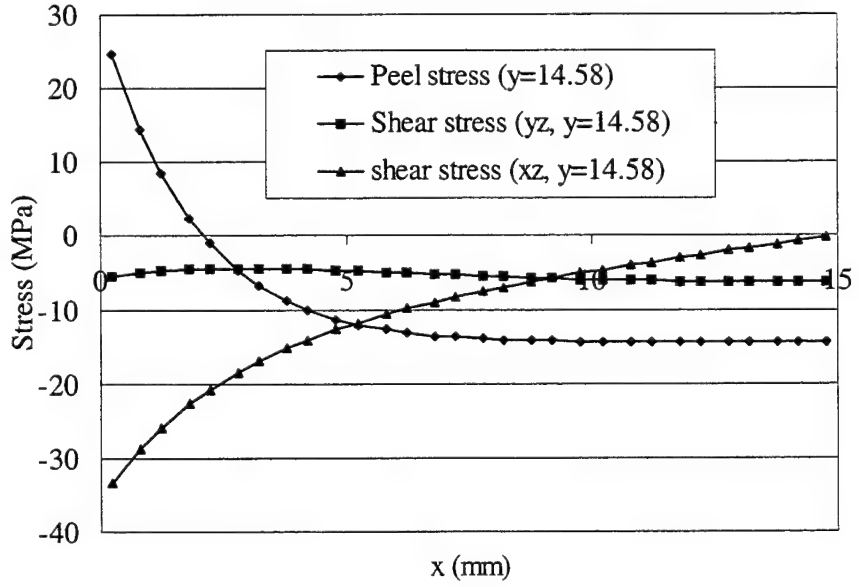

Figure 8-2(b) Thermal stress distribution along x-axis with peak stress for the metallic cylindrical shell with internal metallic patches

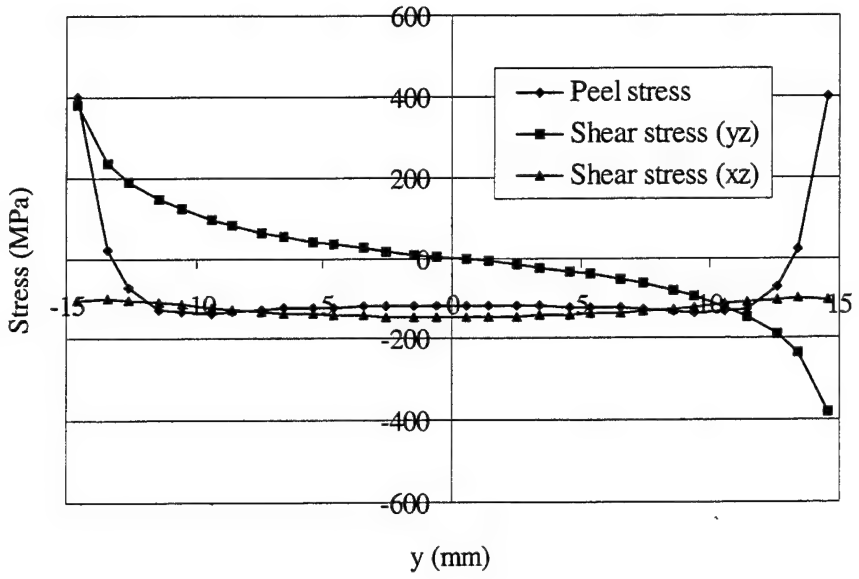

Figure 8-3(a) Thermal stress distribution along y-axis at x=0 for the metallic cylindrical shell with external composite patches

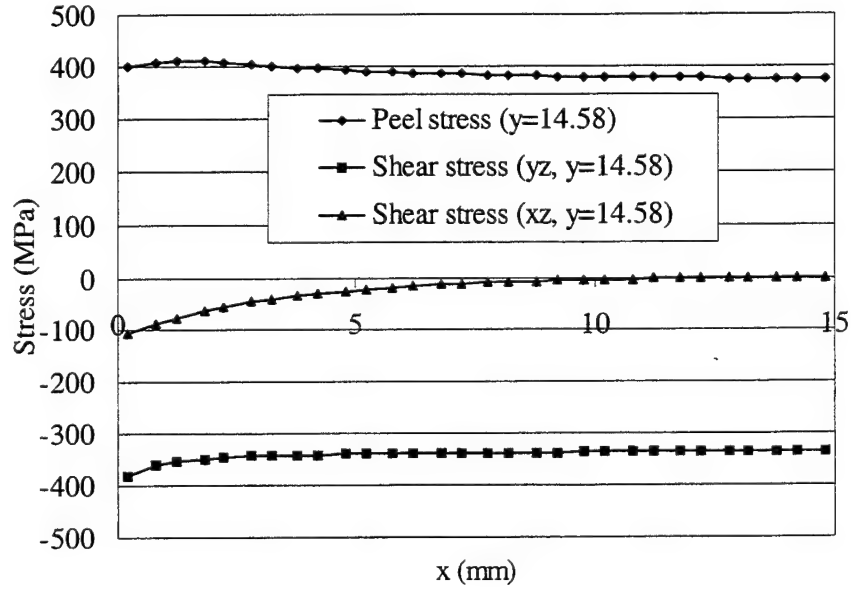

Figure 8-3(b) Thermal stress distribution along x-axis with peak stress for the metallic cylindrical shell with external composite patches

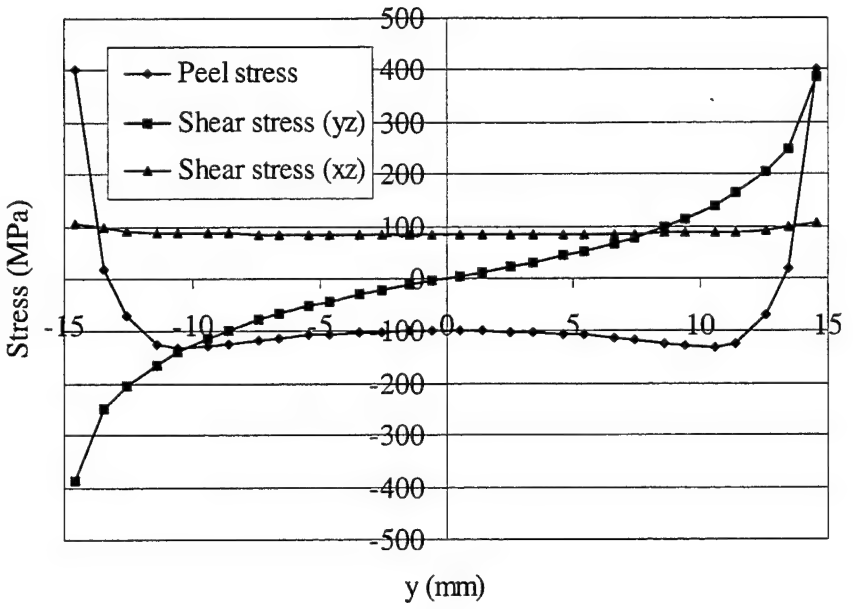

Figure 8-4(a) Thermal stress distribution along y-axis at x=0 for the metallic cylindrical shell with internal composite patches

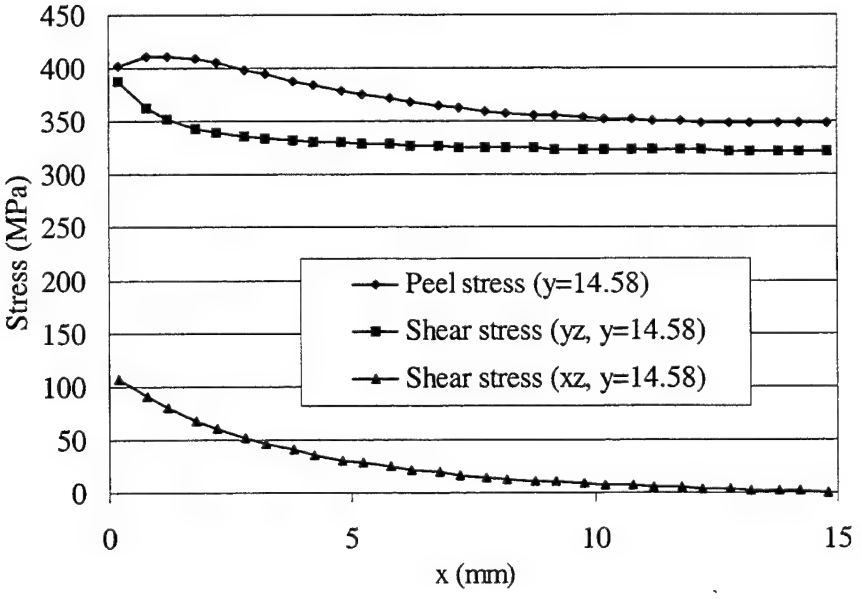

Figure 8-4(b) Thermal stress distribution along x-axis with peak stress for the metallic cylindrical shell with internal composite patches

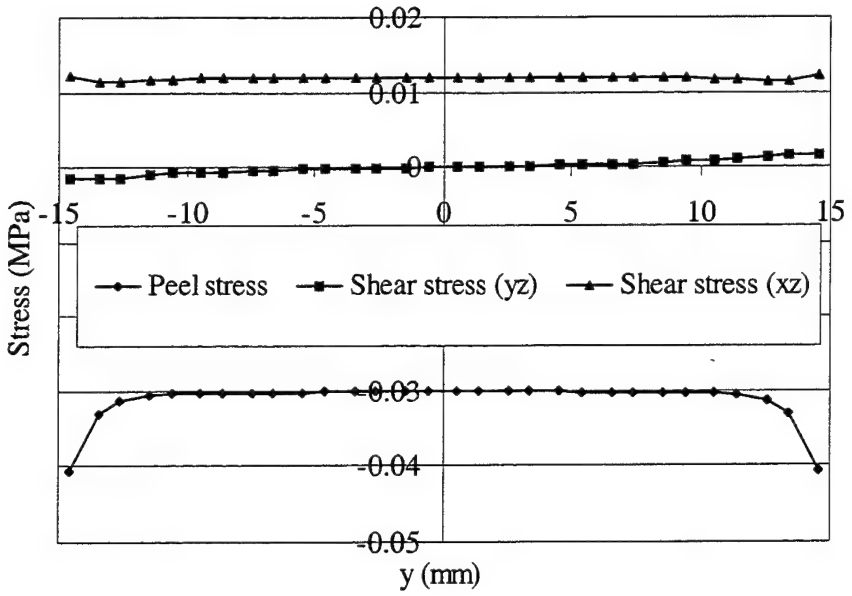

Figure 8-5(a) Thermal stress distribution along y-axis at x=0 for the composite cylindrical shell with external composite patches

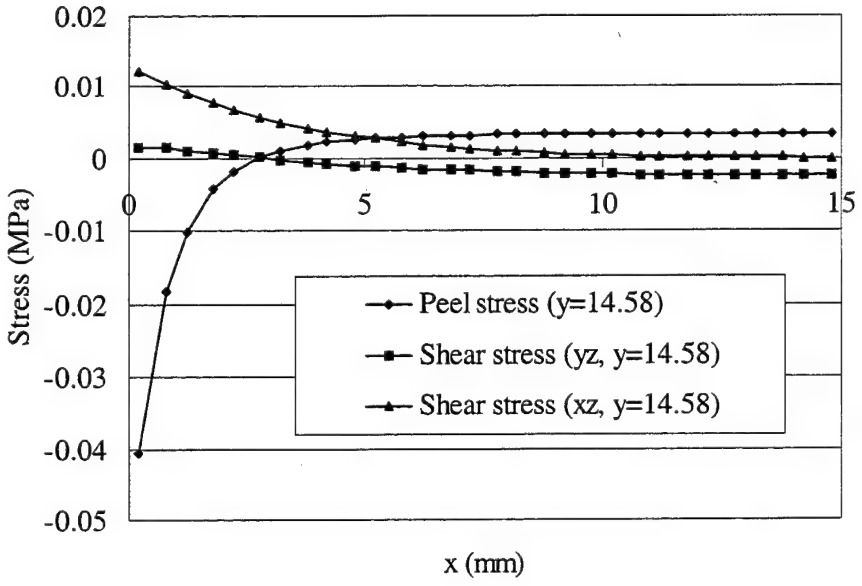

Figure 8-5(b) Thermal stress distribution along x-axis with peak stress for the composite cylindrical shell with external composite patches

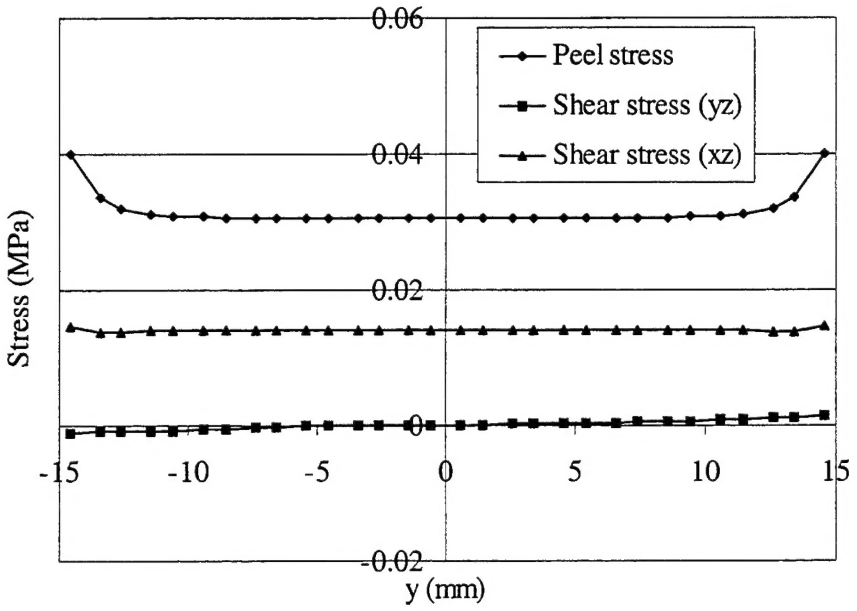

Figure 8-6(a) Thermal stress distribution along y-axis at x=0 for the composite cylindrical shell with internal composite patches

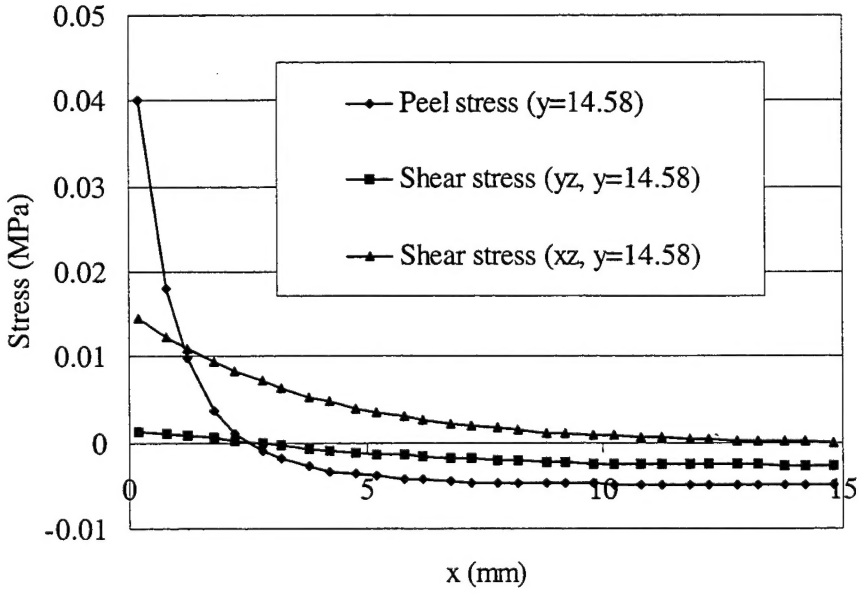

Figure 8-6(b) Thermal stress distribution along x-axis with peak stress for the composite cylindrical shell with internal composite patches

9. CONCLUSIONS

In this report, a novel finite element formulation has been developed for developing 2.5-D adhesive elements. Three adhesive elements, namely, 8-node, 16-nod and 18-node adhesive elements, are developed using the new formulation and then validated by correlating with the results predicted using the commercial finite element software. Both large deflections of parent shell structures and nonlinear adhesive behavior are taken into account in the formulation. Thermal loading is also incorporated in the formulation to enable analysis of bonded repair under a combined mechanical and thermal loading. The newly developed elements can be used to quickly calculate stresses in the adhesive layer of bonded repairs to curved thin-walled structures. The adhesive element provides an efficient and cost-effective means of modeling bonded overlap area in bonded repairs. A large variety of numerical examples have been analyzed to provide an in-depth understanding of the curvature on stresses in adhesive layer. The results from the selected numerical examples demonstrate the following points:

(a) The curvature of a parent structure may have a profound effect on peak stresses in adhesive layer, depending on loading and boundary conditions;
(b) The peak peel and shear stresses may increase or decrease with an increased curvature depending on loading and boundary conditions;
(c) Externally bonded patches seem to create less peak peel stress than internally bonded patches for the cylindrical shells under an internal pressure, while internally bonded patches seem to create less peak peel stress than externally bonded patches for the cylindrical shells under an external pressure; In other words, external patches are preferred when the shell is under an internal pressure while internal patches are preferred when under an external pressure;
(d) Both large deflection and adhesive nonlinear behavior can have a significant influence on the peak values and distributions of the three stresses in the adhesive layer;
(e) External patching is preferred when a cylindrical shell is subjected to a negative temperature change;
(f) The size and thickness of the bonded patch may have an important effect on the peak peel stresses.

ACKNOWLEDGEMENT

The authors wish to acknowledge valuable technical discussions with and encouragement from Drs Greg Schoeppner and Nick Pagano of MLBC/AFRL, Ozden Ochoa of AFOSR and Tom Kim of AOARD/AFOSR. This research was sponsored by AOARD/AFOSR (Contract Number: F6256200M9108).

REFERENCES

1. Baker A A and Jones R. Bonded repair of aircraft structures. Martinus Nijhoff: Dordrecht; 1988
2. Baker A.A., Repair techniques for composite structures, Composite Materials in Aircraft Structures, Middleton D.H., Ed., Longman Scientific & Technical, 1990, Chapter 13, pp. 207-227
3. L.R.F. Rose, A cracked plate repaired by bonded reinforcement, Int. J. Fracture, 18, 135-144, 1982
4. L.J. Hart-Smith, The design of repairable advanced composite structures, Douglas Paper 7550, McDonnell Douglas, Douglas Aircraft Company, 1985
5. Adams R D Comyn J and Wake W C. 1997, *Structural Adhesive Joints in Engineering*, 2nd Edition. Chapman & Hall: London; 1997
6. Tong L and Steven G P. *Analysis and Design of Structural Bonded Joints*. Kluwer Academic Publishers: Boston; 1999
7. Zhu J F and Zheng G. *Shanghai J of Mechanics* 1997; 18: 277-283
8. Zienkiewicz O C and Taylor R L. The Finite Element Method. 4th Ed. Vol. 1 Basic Formulation and Linear Problems. McGraw-Hill Book Company: London; 1989
9. Belytschko, T., Wong B.L. and Stolarski H., Assumed strain stabilzation procedure for the 9-node Lagrange shell element, International Journal for Numerical Methods in Engineering, 1989, Vol.28, 385-414
10. Wong B.L. and Belytschko T., Assumed strain stabilization procedure for the 9-node Langrange plane and plate elements, Engineering Computation, 1987, Vol.4, 229-239
11. Malvern L.E., Introduction to the Mechanics of a Continuum Medium, Prentice-Hall, Englewood Cliffs, N.J., 1969